Quaternary Science Advances 13 (2024) 100156

Contents lists available at ScienceDirect

Quaternary Science Advances

journal homepage: www.sciencedirect.com/journal/quaternary-science-advances

Spatial and temporal variability in Holocene trough-fill sediments, King Haakon Trough System, sub-Antarctic South Georgia

Nina-Marie Lešić [a,b,c,*], Katharina Teresa Streuff [a,b], Gerhard Bohrmann [a,b], Sabine Kasten [a,b,c], Gerhard Kuhn [b,c]

[a] MARUM - Center for Marine Environmental Sciences, University of Bremen, Leobener Straße, 28359 Bremen, Germany
[b] University of Bremen, Faculty of Geosciences, Klagenfurter Straße, 28359 Bremen, Germany
[c] Alfred Wegener Institute Helmholtz Centre for Polar and Marine Research, Am Handelshafen 12, 27570 Bremerhaven, Germany

ARTICLE INFO

Keywords:
Sub-antarctic
South atlantic
Acoustic data
Marine sedimentology
Palaeoreconstruction
Depositional environments

ABSTRACT

The climate in the South Atlantic sector of the sub-Antarctic, and therefore on and around the island of South Georgia, is dependent on the Southern Hemisphere Westerlies (SHW) and the Antarctic Circumpolar Current (ACC). The SHW and the ACC, in turn, are strongly controlled by climate variability in the Southern Hemisphere. Accordingly, thick sediment sequences in the troughs across South Georgia's continental shelf serve as valuable archives for past climate variations in the Southern Ocean. Since Holocene climate fluctuations led to only minimal oscillations in glacier margin positions within the fjords, the entire shelf was exposed to dynamic ocean currents since at least 10 ka BP. Its depositional systems are therefore a suitable target for the reconstruction of Holocene dynamics of both the SHW and the ACC. Sub-bottom profiler data and radiocarbon ages from four gravity cores from the south-western South Georgia continental shelf provide evidence for a complex interplay between island run-off and ocean currents intruding into a unique cross-shelf trough system during the last ~10 ka. The data reveal several prominent changes in sediment and Holocene climate dynamics, the most significant occurring between 8 and 7.7 cal ka BP and between 2.6 and 2.2 cal ka BP. Both of these time periods represent transitions from warmer to cooler and windier conditions in South Georgia and the Southern Hemisphere. Our record from the King Haakon Trough System is the first highly resolved Holocene archive from the marine realm on the south-western South Georgia continental shelf and suggests several large-scale Southern Hemisphere climate changes during the mid-to late Holocene.

1. Introduction

The deposition of marine sediments, especially in previously glaciated areas, depends not only on local and regional climate, glacier dynamics and (associated) terrestrial runoff, but is also influenced by the ocean floor geomorphology and its resulting exposure to cross- and along-shelf currents. The latter can be highly variable and are often intrinsically linked to the presence of, e.g., exposed bathymetric highs or deeply incised glacial troughs, particularly on continental shelves (Dunbar et al., 1985; Dickens et al., 2014, 2019; Graham et al., 2017). In climatically dynamic regions, such as the sub-Antarctic microcontinent of South Georgia (SG), the already complex interplay between ocean, atmosphere and, still partially glaciated, landmasses, is complicated even further by frequent shifts in the predominant climatic systems. Indeed, the interplay between Southern Hemisphere Westerlies and the Antarctic Circumpolar Current fronts (SHW and ACC, respectively, Fig. 1a; Moreno et al. (2018); Orsi et al. (1995)), as well as a wide and exposed shelf, make the entire region vulnerable to changing ocean configuration (cf. Anderson et al., 1984; Dunbar et al., 1985; Nicholls et al., 2009; Graham et al., 2017; Hillenbrand et al., 2017). As a result, (glaci-)marine sediments around the island do not only archive the multitude of processes affecting their deposition, but also the evolution of such processes over time. The thick sedimentary sequences accumulated in the glacially-incised cross-shelf troughs around SG (Graham et al., 2008) are particularly suitable for climate reconstructions, because they provide insights into Holocene climate variability and resulting environmental changes - also in the broader context of Southern Hemisphere atmospheric oscillations - at a high temporal

* Corresponding author. Faculty of Geosciences, University of Bremen, Klagenfurter Str. 2-4, 28359 Bremen, Germany.
E-mail addresses: nlesic@marum.de (N.-M. Lešić), kstreuff@marum.de (K.T. Streuff), gbohrmann@marum.de (G. Bohrmann), sabine.kasten@awi.de (S. Kasten), ge_ku@uni-bremen.de (G. Kuhn).

https://doi.org/10.1016/j.qsa.2023.100156
Received 29 August 2023; Received in revised form 4 December 2023; Accepted 7 December 2023
Available online 13 December 2023

resolution.

Despite its potential for climate research, data on the SG micro-continent is mostly restricted to the island itself. Most studies investigating Holocene climate records (after 11.7 ka; Walker et al., 2009), have focused on a small area of the terrestrial north-eastern part of the island (e.g. Clapperton et al., 1989; Rosqvist et al., 1999; Rosqvist and Schuber, 2003; van der Putten et al., 2004; van der Putten and Verbruggen, 2005; van der Putten et al., 2009; Oppedal et al., 2018; Berg et al., 2019; Zwier et al., 2021; van der Bilt et al., 2022), while only two studies exist on the southern side of SG (Strother et al., 2015; Foster et al., 2016). Even fewer studies investigate the marine environment, where, to our knowledge, the only climate archive that focuses on the Holocene has been documented from a coastal inlet in Cumberland Bay, also located in north-eastern SG (Berg et al., 2019).

This study presents, for the first time, hydroacoustic data in combination with radiocarbon ages of sediments from a large cross-shelf trough system, the King Haakon Trough System (KHTS; Fig. 1). The aim is to investigate marine Holocene climate records from the south-western SG continental shelf. Apart from presenting and interpreting the Holocene acoustic record, it seeks to correlate sedimentological signatures observed from the local marine environment with climate events from other SG records and the Atlantic sector of the Southern Ocean. Our dataset is the first highly resolved Holocene record from the marine environment south of SG. It does not only show repeated changes in KHTS sedimentation consistent with regional Holocene climate variability, but also demonstrates that depositional environments, even in the inner-shelf regions, were influenced by large-scale Southern Hemisphere-related processes (Bentley et al., 2009; Voigt et al., 2015; Moreno et al., 2018; Berg et al., 2019; Zwier et al., 2021; van der Bilt et al., 2022).

2. Study area

2.1. Physiographic setting

SG is located in the South Atlantic (54–55° S, 35.5–38°W; Fig. 1) and is one of the few large islands in the sub-Antarctic (Gordon et al., 2008; Berg et al., 2019). It is not only positioned within the core of the SHW belt (Fig. 1a), but also between two primary fronts of the ACC, i.e. the present-day Polar Front (PF) and the Southern Antarctic Circumpolar Current Front (SACCF), with the latter tracing the northern continental shelf break (Fig. 1a) (Orsi et al., 1995; Thorpe et al., 2002; Matano et al., 2020; Combes et al., 2023). These circumpolar fronts are ~20,000 km long and show enhanced latitudinal water property gradients across the entire water column. Despite their mostly simplified depiction as the main (isolated) jets of ACC transport, they actually consist of several intertwined branches, thus forming an extensive jet structure in many areas (Sokolov and Rintoul, 2009; Matano et al., 2020; Combes et al., 2023). This is also the case around SG, where a branch of the SACCF directly borders the south-western shelf edge (Fig. 1b). The SACCF intrudes onto the shelf in the area of KHTS, where, amplified by wind stress, it affects cross-shelf transport (Combes et al., 2023). In consequence, SG's position within these atmospheric and oceanographic systems makes the island and its continental shelf, including its sedimentary systems, sensitive to changes in position and strength of both SHW and ACC over time (cf. Strother et al., 2015; Graham et al., 2017;

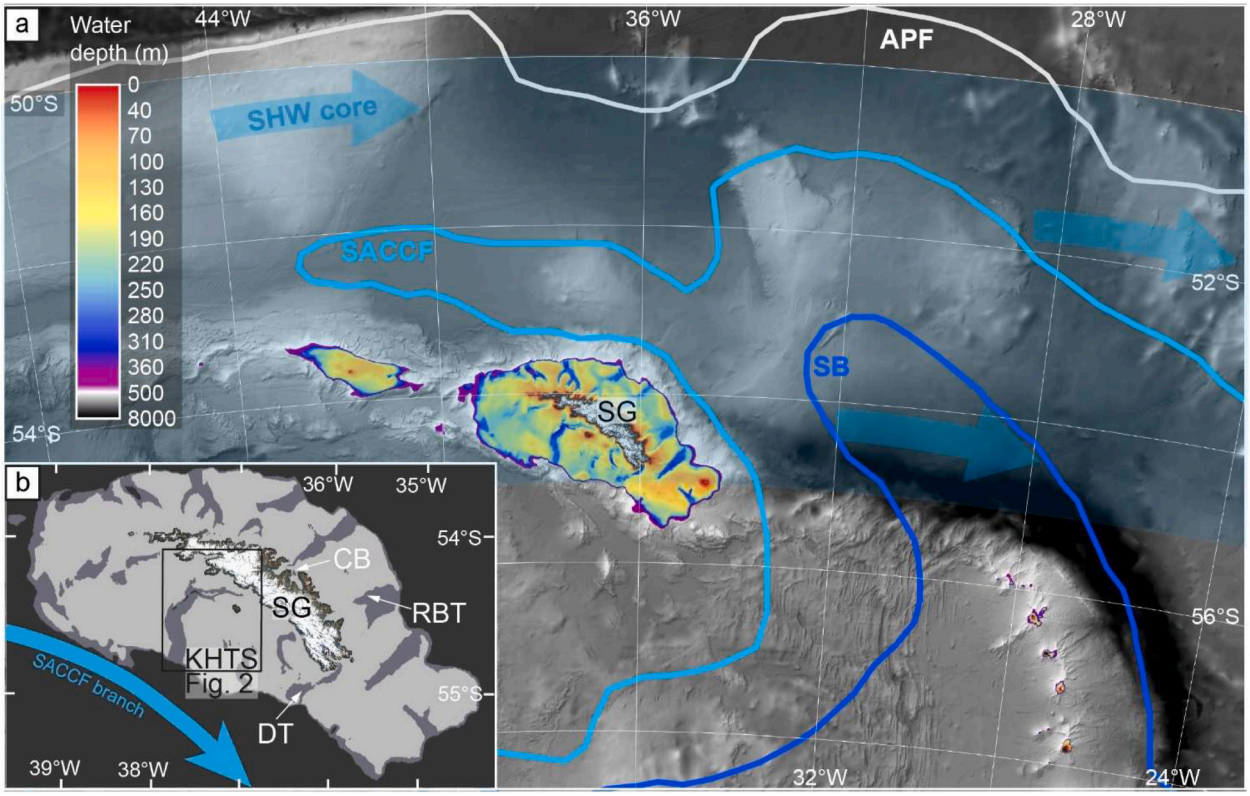

Fig. 1. a) Location of South Georgia (SG) with respect to the core belt of the Southern Hemisphere Westerly Winds (SHW; 50–55°S; blueish shading and blue arrows; Lamy et al. (2010)) and three of the major oceanographic Antarctic Circumpolar Current (ACC) fronts in the Southern Ocean. PF = Polar Front, SACCF = Southern Antarctic Circumpolar Current Front, and SB = Southern Boundary of the ACC, their positions inferred from Orsi et al. (1995). b) Broad overview of the SG shelf morphology and an adjacent SACCF branch (adapted after Matano et al., 2020). Dark grey areas show the numerous, likely glacially-incised, cross-shelf troughs, e.g. Drygalski Trough (DT) and Royal Bay Trough (RBT; >250 m water depth). The location of King Haakon Trough System (KHTS) is shown by a black rectangle that also shows the extent of Fig. 2. Light grey areas on the shelf show water depths <250 m, including Cumberland Bay (CB; Graham et al., 2017). DEM information for the shelf and surrounding ocean is based on GEBCO Compilation Group (2023), while map information for the island derives from Landsat imagery provided by South Georgia GIS (2023). (For interpretation of the references to colour in this figure legend, the reader is referred to the Web version of this article.)

Moreno et al., 2018; Matano et al., 2020; Bakke et al., 2021; Yamazaki et al., 2021).

KHTS is located between 54°08′ and 54°50′S and 37°14′ and 37°39′W, on the SG continental shelf. It is bordered by the south-western SG coast to the north-east, Annenkov Island to the east and the continental shelf edge to the south (Fig. 2). It is closely associated with the Cooper Bay Shear Zone (CBSZ, Fig. 2b), a large fault complex, which divides rock formations on land and is inferred to continue onto the continental shelf, likely passing through the KHTS tributaries. The trough system consists of a main trough on the mid- and outer shelf, i.e. King Haakon Trough (KHT, Fig. 2b), an adjoining smaller trough system on the inner shelf, which we define as the Jacobsen Trough System (JTS), to the east, and some additional, albeit smaller, arms and feeding systems. KHT strikes north-south (Fig. 2a) and is connected to the coast by the shallower conjoined Cheapman and King Haakon Bays, from here on referred to as King Haakon Bay (Fig. 2; Hodgson et al., 2014). King Haakon Bay is mostly fed by the Briggs tidewater Glacier and extends first E-W, then N–S, before it joins KHT on the inner continental shelf (Fig. 2a).

JTS is composed of two main troughs, Jacobsen Trough (JT, ~22.5 km long) to the north and Annenkov Trough (AT; ~28 km long with tributaries) to the south, both of which strike east-west and are separated by a prominent bedrock feature (Fig. 2; unofficially named in Bohrmann et al. (2017)). For easier identification, we subdivide JT into an eastern, a central, and a western part (Fig. 2a, A.1). East JT represents the junction of JT with both the 3.4-km-wide Jossac Bight and the Jacobsen-Newark Tributary, an around 5-km-wide, ESE-WNW striking and ~23-km-long tributary composed of Newark Bay and Jacobsen Bight (Fig. 2a), which likely follows the CBSZ (Fig. 2b). Central JT marks the initial separation of JTS into JT and AT, while west JT includes the deepest parts of JT and extends all the way to the confluence with KHT (Fig. 2). According to patchy bathymetric data towards the coast, JTS is fed by multiple fjords and bays, all of which are outlets for an array of marine-terminating tidewater glaciers (Fig. 2; U.S.G.S., 1981; Gordon

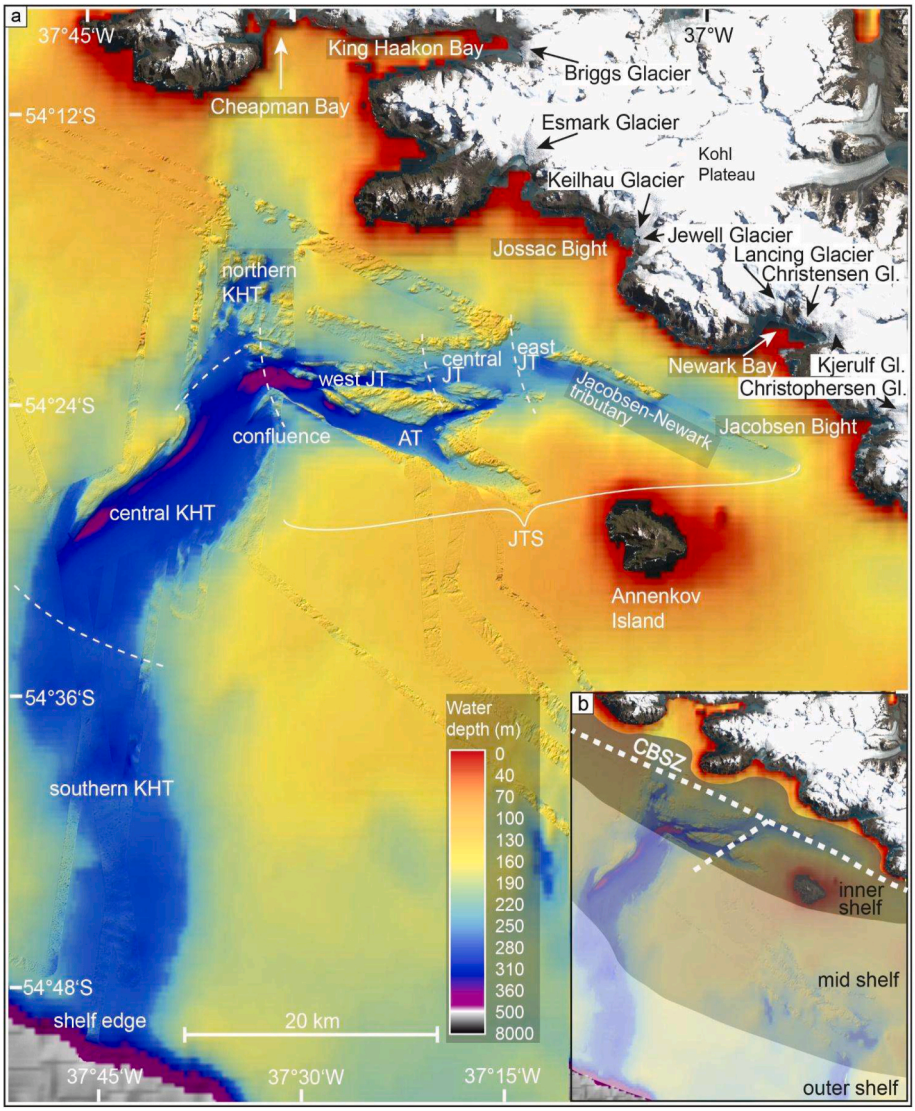

Fig. 2. a) Overview of the bathymetry of the King Haakon Trough System and the glaciers within its catchment area. In addition to the main trough, King Haakon Trough (KHT), Jacobsen Trough (JT) and Annenkov Trough (AT) are the predominant tributaries, which, in turn, are joined by Jossac Bight from the north and the Jacobsen-Newark tributary from the east. AT and JT together with their tributaries form the Jacobsen Trough System (JTS). JT is subdivided here into an eastern, a central and a western part. b) Visualisation of the different shelf areas referred to in the manuscript, including inner shelf (comprising King Haakon Bay, Cheapman Bay, and JTS with all tributaries), sediment-rich mid-shelf (comprising central KHT), and sediment-starved outer shelf (comprising the distal part of KHT until the shelf edge). The inner shelf and the eastern part of JTS are cross-cut by the inferred extension of the Cooper Bay Shear Zone (CBSZ; modified after Macdonald et al., 1987) and Dalziel et al. (2021), also referred to as Cooper Bay Dislocation Zone.

et al., 2008; Cook et al., 2010).

3. Methods

Hydroacoustic data, acquired on cruise M134 with *RV Meteor* in 2017 (Bohrmann et al., 2017), were complemented with radiocarbon dates from four sediment cores, and used to analyse the regional Holocene depositional environments in KHTS (Fig. 3). While this paper focuses on sediment echosounder data from the Holocene, two forthcoming papers will concentrate on (i) the detailed core lithologies and associated local environments and (ii) the pre-Holocene glacial history.

Bathymetric data were collected using a Kongsberg Maritime EM710 multibeam echosounder with 432 beams for water depths <500 m, and a Kongsberg Maritime EM122 with 256 beams for water depths exceeding 500 m. The shallow-water echosounder was operated at a frequency between 70 and 100 kHz, the deep-water echosounder at a nominal frequency of 12 kHz. Bathymetric data were processed using MB-System Suite (Caress and Chayes, 2017), gridded to a resolution of 5 m, and visualised and interpreted with the software QGIS 3.22.11.

Sediment echosounder data were collected with a parametric Teledyne ATLAS PARASOUND P70 sub-bottom profiler. The system was operated at a secondary low frequency of ~4 kHz. The data were visualised and interpreted using SMT The Kingdom Suite 2019. Interpretations for this study were restricted to seven profiles, 1–7, deemed representative for the entire trough system (Fig. 3). All hydroacoustic systems were frequently calibrated during data acquisition using sound velocity profiles and repeated Conductivity-Temperature-Depth measurements. All depth conversions are based on an assumed average sound velocity of 1500 ms^{-1} within the sediments (Figs. 4–6, 8, Table 2).

For stratigraphic information on the sub-bottom profiles, radiocarbon dating was performed on samples from four gravity cores. Cores GeoB22056-1, GeoB22057-1, and GeoB22058-1 were taken from JT during the *RV Meteor* cruise M134 in 2017 (Fig. 3; Bohrmann et al., 2017), while core PS133/2_17–13 was taken from central KHT during the *RV Polarstern* cruise PS133/2 in 2022 (Kasten, 2023). All core information is summarised in Table 1.

Crude lithofacies logs allowed for the correlation with acoustic data

Table 1
Core information for the gravity cores GeoB22056-1, GeoB22057-1 and GeoB22058-1 taken during expedition M134, as well as core PS133/2_17–13 taken during expedition PS133-2, respectively.

Core Name	Latitude	Longitude	Water Depth [m]	Recovery [cm]
GeoB22056-1	54°23.003′ S	37°14.142′ W	259	722
GeoB22057-1	54°23.024′ S	37°16.970′ W	266	879
GeoB22058-1	54°23.043′ S	37°19.388′ W	268	941
PS133/2_17-13	54°24.078′ S	37°34.031′ W	344	895

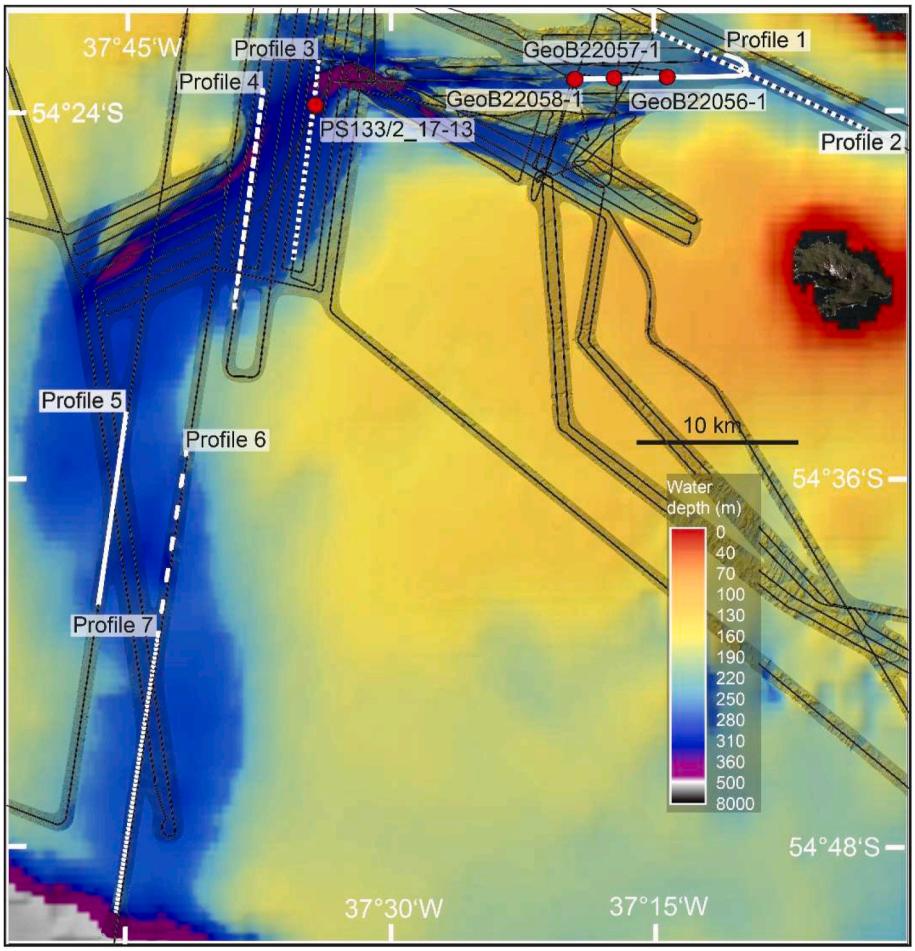

Fig. 3. Overview of the data, including the extent of high-resolution bathymetric and sub-bottom profiler data (transparent grey polygon and black lines, respectively), the location of the seven sub-bottom profiles shown in this study (white Profiles 1–7), and the four sediment cores (GeoB22056-1. GeoB22057-1, GeoB22058-1 and PS133/2-_17–13).

Table 2
Characteristics of the four subunits of AF2 in stratigraphic order.

Unit	Acoustic character	Distribution	KHT Thickness	JT Thickness
D	continuous, perfectly parallel mostly horizontal reflector, medium to high amplitude	Draping	2–4	4–15
C	Weak stratification, higher amplitude & higher impedance in JT	Pinches out towards bathymetric highs	1–10 m	0-> 30 m
B	Weak stratification, semi-transparent	Conformably overlies A in most parts, pinches out towards bathymetric highs in KHT	1–8.5 m	0->27
A	Distinct stratification	Widespread	6–48 m	8–35 m

and the identification of distinct lithological boundaries, interpreted to represent acoustic unit boundaries. Biogenic carbonate was isolated from >63 μm sample fractions and the sediment surface of the split core halves above and below these boundaries as well as at the core base and was sent for Accelerator Mass Spectrometry (AMS) ^{14}C dating as CO_2 samples at the MICADAS laboratory at AWI (Mollenhauer et al., 2021). Lab errors are between ±0.036–0.108 ka. Radiocarbon age calibration was carried out with the IntCal20 calibration curve (Reimer et al., 2020), using modelled Marine Reservoir Ages (MRA; Butzin et al., 2019) with a temporal resolution of 0.05 ka that are based on three simulations. Their median absolute deviations (MAD) lie within the laboratory error and are therefore neglected (cf. Butzin et al., 2019; Butzin et al., 2020; Heaton et al., 2020; Heaton et al., 2022). All boundary-specific ages were taken within a maximum vertical distance of 20 cm from the lithological boundaries, except in core PS133/2_17–13, where a sample at 434 cm was taken 126 cm below the respective boundary. All obtained ages lie (within their errors) in the expected stratigraphic order and are based on a variety of biogenic carbonate, rather than just foraminifera. Accordingly, we consider the ages reliable, despite the fact that radiocarbon dating and calibration, especially on foraminifera, can be difficult in polar oceans (cf. Heaton et al., 2022) and the SG region (Berg et al., 2020). All ages are presented in calibrated kiloyears before present (cal ka BP; see Tables 3 and 4 in section 4 below).

Table 4
Average linear sedimentation rates for the Units A-D based on the ages provided in Table 3. Note that these simple sedimentation rates assume that 0 cm in the core represents recent sedimentation and are rates for unit D are therefore only estimated.

Core	Unit	Thickness (cm)	Time period (ka)	Sedimentation rate (cm ka^{-1})	Sedimentation rates A and (B + C + D)
GeoB22056-1	D	645	1.483	435	435
GeoB22057-1	D	430	2.598	166	93
GeoB22057-1	B	110	3.23	34	
GeoB22058-1	D	380	2.143	177	177
GeoB22058-1	A	370	2.449	151	151
PS133/2_17-13	D	183.5	2.557	72	73
PS133/2_17-13	C	120	1.587	77	
PS133/2_17-13	A	451.5	0.517	873	873

4. Results and interpretation

4.1. Trough morphology

4.1.1. Description

The mapped extent of KHT, which we separated into a northern, central and southern part (Fig. 2a), is approximately 70 km long, up to 10 km wide and shoals from its deepest part, at the confluence between central KHT and JTS (401 m; Fig. 2a), to ~275 m at the shelf edge. In contrast, JTS, with all its mapped tributaries, is ~74 km long, up to 4 km wide, with shallow, rugged flanks (<200 m) and some deeper central basins (Fig. 2a). A small bedrock high splits west JT into a shallower northern (<240 m) and a deeper (370–401 m) southern arm. The presence of several shoals creates a funnel-like geometry around the boundary of central and west JT, causing it to narrow and constrict into a bottleneck shape just before joining KHT (Fig. 2a). AT on the other hand is relatively uniform in width (~2 km), but similar in depth (200–370 m; Fig. 2). AT's deepest part is marked by a bathymetric depression at a water depth of 370 m, close to the conjuncture with west JT (Fig. 2a).

The high-resolution bathymetric data show that KHTS is characterised by a smooth seafloor in the majority of its trough valleys,

Table 3
Conventional radiocarbon ages and calibrated weighted mean ages (cal ka BP) from the four sediment cores discussed in the text. Note that the Unit boundaries are up to 12 cm thick in the cores.

Sample details			Conventional radiocarbon ages		IntCal20 calibration	*Unit*	*Vertical distance to Units Boundaries (cm)*	Lab Code
Gravity core	Depth (cm)	Carbon (ate) source	Age(^{14}C ka BP)	Age error (ka)	Weighted mean(cal ka BP)			
GeoB22056-1	645	Mollusc	2.504	±0.06	1.483	D	–	AWI 4455.1.1
GeoB22057-1	430	Mollusc	3.403	±0.066	2.598	D	4 cm above C-D boundary	AWI 4458.1.1
GeoB22057-1	460	Mollusc	4.443	±0.067	3.899	B	14 cm below B-D boundary	AWI 4459.1.1
GeoB22057-1	750	Mollusc	7.285	±0.079	7.129	B	304 cm below B-D boundary	AWI 4463.1.1
GeoB22058-1	380	Bryozoa	2.983	±0.062	2.143	D	20 cm above A-D boundary	AWI 6171.1.1
GeoB22058-1	430	Benthic Forams	7.879	±0.087	7.718	A	18 cm below A-D boundary	AWI 4465.1.1
GeoB22058-1	800	Benthic Forams	9.896	±0.09	10.167	A	388 cm below A-D boundary	AWI 4470.1.1
PS133/2_17-13	183.5	Mollusc	3.323	±0.062	2.557	D	13.5 cm above C-D boundary	AWI 10474.1.1
PS133/2_17-13	303.5	Mollusc	4.65	±0.073	4.144	C	1.5 cm above A-C boundary	AWI 10476.1.1
PS133/2_17-13	434	Benthic Forams	8.696	±0.084	8.511	A	126 cm below A-C boundary	AWI 10477.1.1
PS133/2_17-13	885.5	Fish scale	9.038	±0.036	9.028	A	582 cm below A-C boundary	AWI 10480.1.1

especially within JTS (Fig. 2a) and in central KHT (Fig. 2a). The most prominent feature are elongated depressions, which are orientated parallel to the trough flanks, and occur close to the confluence zones of tributaries and troughs (Fig. 2a) and along the western flank of KHT (Fig. 3a). They are ~1–6 km long and exceed 360 m water depth, meaning they are overdeepened with respect to the remaining trough system. Shallower areas of the trough (<300 m), such as flanks and bathymetric highs, have a rugged appearance and host some moraines and glacial lineations, which were previously identified in Graham et al. (2008).

4.1.2. Interpretation

The contrast between smooth trough basins and the rugged surrounding seafloor indicates increased sediment accumulation and associated obliteration of the palaeo-relief within the trough basins. Accordingly, these basins probably served as sediment traps in KHTS, where a variable depth of the seafloor might be related to spatially variable sedimentation rates. Nonetheless, deeper trough parts, such as in west JT and around the confluence zone with KHT, may also represent locally enhanced erosion along preferential water/ice pathways. Likewise, the prominent elongate depressions along the western flank of KHT are possibly formed from focused and potentially accelerated flow. Since they are somewhat comparable to subglacial meltwater channels (e.g. Nitsche et al., 2013; Kirkham et al., 2020), tunnel valleys (e.g. Ó Cofaigh, 1996; van der Vegt et al., 2012; Kirkham et al., 2022), canyons (e.g. Inman et al., 1976) or deep-sea trough settings (e.g. Stow et al., 2002), feasible erosion agents could be streaming ice, subglacial meltwater, directed bottom-currents, or a combination of the three. Based on correlation with the sub-bottom profiler data (see section 4.2 below), however, we interpret the bathymetric depressions as 'moats' and the adjacent sediment bodies as 'mounded drifts' after Rebesco et al. (2014).

4.2. Acoustic units

4.2.1. Description

The seven sub-bottom profiles from KHTS show three acoustic facies: The acoustic basement (AB), and two overlying acoustic facies, AF1 and AF2. Because AB and AF1, both consecutively referred to as pre-basin-fill sequence, are subject of a forthcoming paper, this study focuses exclusively on the Holocene trough-fill sequences, AF2. AF2 conformably overlies and onlaps onto the underlying pre-basin-fill sequence (Fig. 5c,e). It effectively fills the topography in the majority of KHTS basins, except on the outer shelf (Fig. 6f). AF2 is at least 80 m thick in east JT (Fig. 2a and 4), but significantly thins to 10–30 m towards central JT. In central KHT, AF2 is significantly thinner, decreasing from 52 to 24 m on the mid-shelf (Fig. 5), to 13 m on the outer shelf (Fig. 6b–e), and negligible amounts at the continental shelf edge (Fig. 6f). AF2 is often influenced by acoustic blanking, which is commonly related to the presence of gas in the sub-surface (Römer et al., 2014; Geprägs et al., 2016). Where acoustic blanking occurs, the overlying reflectors are often enhanced, strongly opaque, and prone to upwards doming (Fig. 4b,d).

AF2 is acoustically stratified, with generally well-defined, parallel internal reflections of variable amplitude. Based on clearly defined reflectors between stratified sequences, as well as vertically variable degrees of stratification, AF2 is subdivided into Units A-D, which show significant variability in thickness. Their characteristics are summarised in Table 2. AF2 was sampled by all four cores in KHTS and consists of fine silty mud.

Unit A occurs in central KHT and in central JT (Figs. 4,5). Although its thickness is variable between 6 and 48 m, its distribution across KHTS is relatively similar. Unit A is thinnest within the moats, but is thickest along mound features commonly found adjacent to the moats. While the sub-bottom profiler data show that the depressions already originated in the pre-basin fill sequence and are characterised by converging reflectors within Unit A, reflectors diverge within their bordering mounds. Moreover, several of Unit A's upper reflectors are locally truncated (Fig. 4c and 5c,e). Unit A was sampled by cores GeoB22058-1 and PS133/2_17–13 and is the only unit that contains frequent diatom-layers intercalated into the very fine silty mud.

Unit B is mainly present in central and east JT and on the mid-shelf around the confluence zone of JTS and KHT (Fig. 4; 5 b-e). Where visible, it overlies older sediments in basins and bathymetric depressions and pinches out towards bathymetric highs in KHT (Fig. 5c,e). It is generally much thinner on the mid-shelf (<8.5 m) than on the inner shelf, where it progressively thins westwards from ~27 m in east JT/the Jacobsen-Newark tributary to 7 m at the location of GeoB22057-1 (Fig. 4c). In central JT, Unit B directly underlies Unit D with local cut-off of its reflectors (Fig. 4c).

Unit C occurs everywhere on the inner shelf, but is locally absent from the stratigraphic record (Figs. 4–6). Its thickness progressively decreases in a westward direction from a maximum of >30 m in east JT to a minimum close to the core location of GeoB22057-1, where it pinches out (Fig. 4b and c). Unlike Units A and B, Unit C does not show truncated reflectors in central JT, but pinches out towards bathymetric highs and flanks in central KHT (Fig. 5c,e). Units B and C form a new, small mound atop an already existing one near the confluence zone of JT and KHT (Fig. 5c), which progressively migrates towards the northwestern flank of KHT.

Unit D is the uppermost acoustic unit and drapes almost the entire trough system except for the outer shelf (Figs. 4–6). Its thickness decreases from 15 m in the JTS tributaries to ~4 m in central JT (Fig. 4c,e), which is also the average thickness in KHT (Fig. 5c,e). Its distinct and opaque basal reflector, *R1,* is characterised by high continuity across the entire trough system and a higher amplitude in JTS than in KHT (Fig. 4b, d; 5 b,d). Unit D directly overlies the acoustic basement on bathymetric highs (Fig. 5c), Unit A in central KHT (Fig. 5d) and east of the bottleneck in central JT (Fig. 4c), as well as Unit B in central JT (Fig. 4c).

4.2.2. Interpretation

Based on its mostly conformable, draping geometry and the stratified appearance, AF2 is interpreted as basin-fill sediment (Ó Cofaigh et al., 2016). On previously glaciated continental margins, such deposits may originate predominantly from (glaci-)marine hemipelagic suspension rainout from turbid meltwater plumes and the water column. Sedimentation can be periodically interrupted by ice rafting, downslope and current-induced re-sedimentation processes, as well as (seasonal) changes in primary production (e.g. Seramur et al., 1997; Forwick et al., 2010; Dowdeswell and Vásquez, 2013; Ó Cofaigh et al., 2016).

Although the acoustic appearance of Units A-D is generally similar, the clearly defined boundaries of the four sub-units suggest episodic changes in the depositional environment across the entire trough system. Moreover, the variably pronounced stratified appearance indicates frequent impedance contrasts, probably caused by the intercalation of at least two different lithologies. In this context, weaker stratification may be related to the interbedding of strata with more similar physical properties. Indeed, the stronger stratification of Unit A may accordingly be caused by the frequent distinct diatom layers intercalated into the otherwise relatively homogeneous mud. This interpretation is consistent with the acoustic signal of glacimarine sediments in Royal Bay Trough (RBT; Fig. 1b), where strong stratification in the lower stratigraphic sequences was also correlated with the occurrence of individual diatomaceous ooze layers (Graham et al., 2017).

Aside from changes in sediment characteristics over time, the variable thickness of Units A-D also implies spatial/temporal variation in sediment accumulation across a larger scale (Fig. 7). The conceptual model in Fig. 7 shows that (i) sediment cover strongly increases from a negligible amount in outer KHT to up to 78 m on the inner shelf in east JT, (ii) sediment sequences are thicker in bathymetric basins than on the shallow banks, and (iii) Units B to D are significantly thicker in JT than in the entire KHT (Fig. 7). Furthermore, shifts seem to have occurred from a more widespread and even deposition (Unit A) to a more

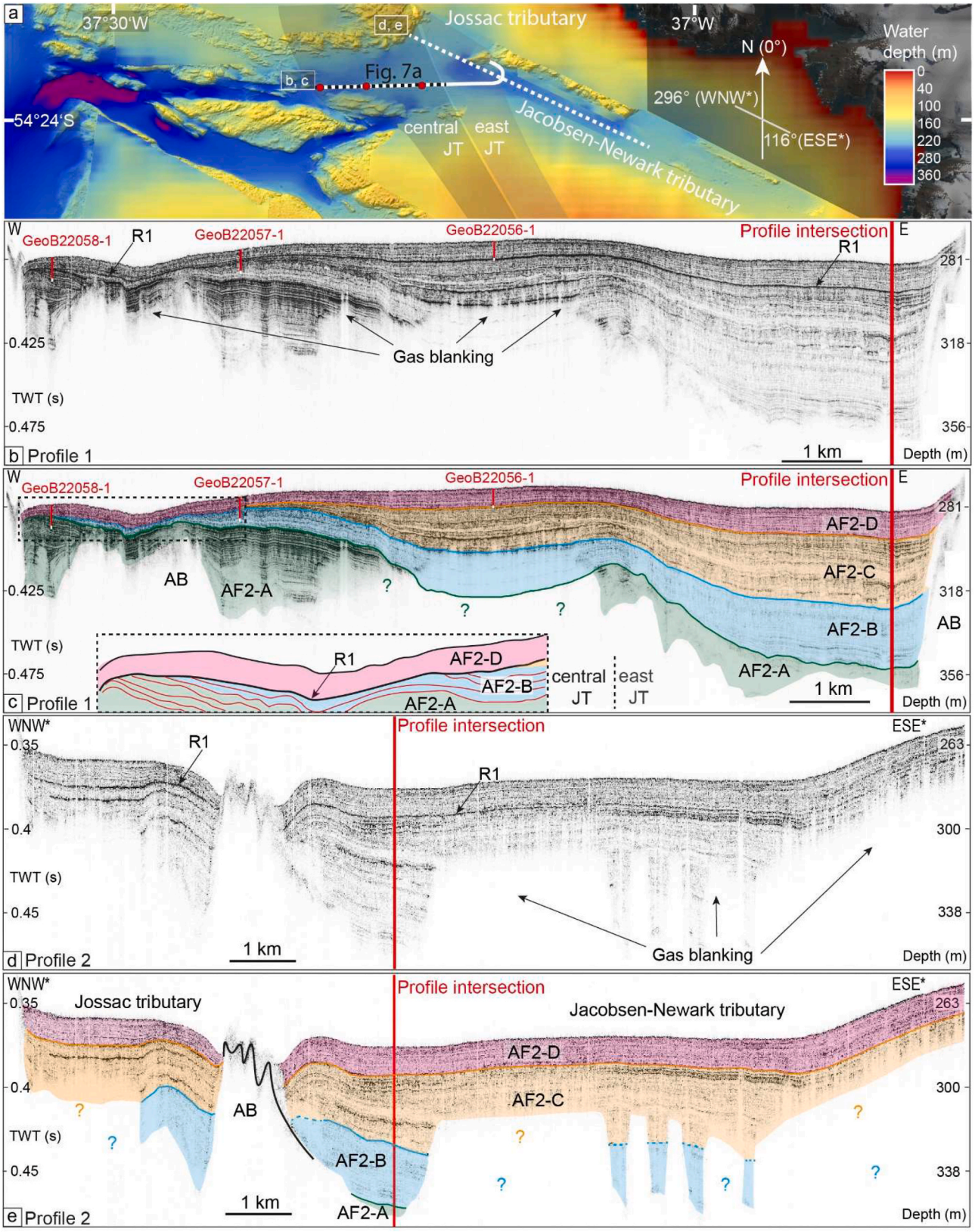

Fig. 4. a) Overview of the position of the sub-bottom profiles in JT, Profiles 1 and 2. b, d) Profile 1 with core locations indicated in red solid lines. White intervals at the bottom of the cores show the estimated true core recovery when accounting for 16% sediment compression. Red vertical lines show the position where Profiles 1 and 2 intersect. c) interpretation of acoustic units in Profile 1. AB = Acoustic Basement, AF2 = basin-fill. AF2-A to D mark the acoustic sub-units of AF2. The inset shows a zoom-in to the unconformity in west JT, demonstrating the presence of cut-off reflectors. d,e) Analogous to b,c) but for Profile 2. Gas blanking is present and affects the mapping of acoustic units in all profiles. (For interpretation of the references to colour in this figure legend, the reader is referred to the Web version of this article.)

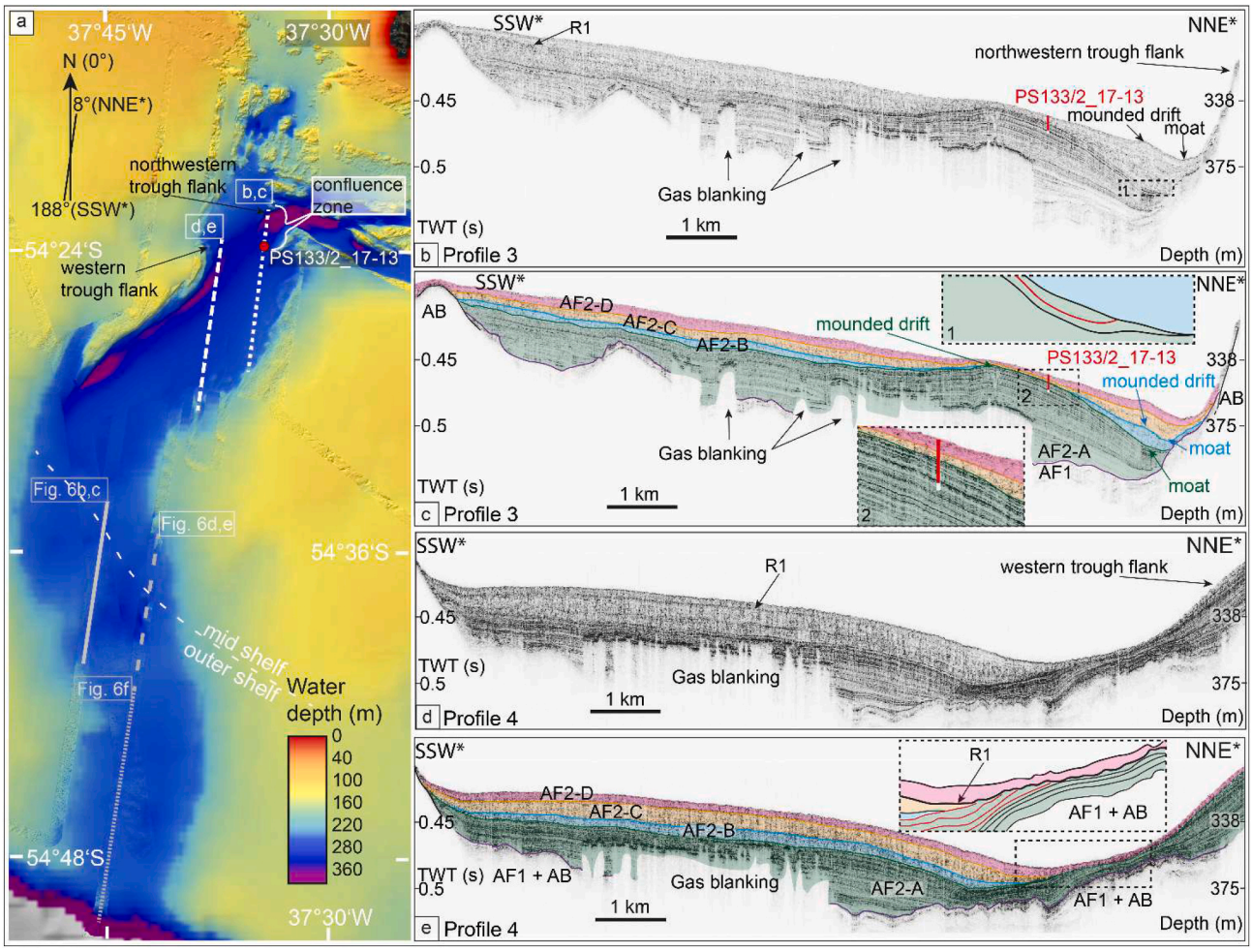

Fig. 5. a) Overview of the position of the sub-bottom profiles in KHT and the core location of PS133/2_17–13. b) Mid-shelf Profile 3 with its stratigraphic interpretation in c). Black dashed rectangle (in b) shows the location of inset 1, while the arrowed R1 refers to a prominent reflector at the base of Unit D. Inset 1 in c) illustrates a truncated reflector of Unit A (red line). Inset 2, illustrated by black dashed rectangles in c) shows a zoom-in to the core location PS133/2-17-13 and the respective unit interpretation. d) Mid-shelf Profile 4 with its stratigraphic interpretation in e). The inset in e) outlined by two black dashed rectangles, shows truncated reflectors of Unit A (red lines). AB + AF1 form the pre-basin-fill sequence and are subject of a forthcoming paper. AF2 in all sub-panels refers to the trough fill, with AF2-A to D representing the acoustic sub-units of AF2. (For interpretation of the references to colour in this figure legend, the reader is referred to the Web version of this article.)

restricted deposition on the inner shelf and within depressions (Units B and C), to trough-wide draping (Unit D). This suggests that not only the main sedimentary processes but also their magnitude within the troughs were subjected to a number of potential factors throughout the Holocene, which will be discussed in detail in section 5.2.

Truncated upper reflectors (Figs. 4c and 5,e), as well as the stratigraphic relationships between Units A, B and D in central JT and western KHT, provide evidence for erosion on a larger scale and an associated stratigraphic unconformity (Figs. 7 and 8). In KHT, Unit A forms the lower, "pre-erosion", part, while Unit D forms the upper "post-erosion" sequence of this unconformity above reflector *R1* (Figs. 4, 5 and 7). In JT, Unit A and B show truncated reflectors and thus both constitute the unconformity's lower part (Fig. 7). In contrast, the fact that Unit D directly overlies the pre-basin-fill sequence in central KHT, is probably related to steeply dipping bedrock (Fig. 5c) preventing the preservation of thick sediment accumulations rather than to erosion from bottom-currents.

In contrast to the more widespread variability in sediment distribution, small-scale differences in sediment deposition are also apparent from the moats and adjacent mounds along the (north)-western flank of KHT (Fig. 5b–e). The internally diverging and converging reflectors, mostly within Units A and C, imply elevated and decreased sediment accumulation, respectively, occurring simultaneously in close spatial association. The combination between erosion and deposition between the observed moats and mounds is typical for bottom-current related contourites and associated moat-drift systems (Wilckens et al., 2023), which supports our previous interpretation of the elongate bathymetric depressions as moats. Accordingly, the adjacent sediment bodies are suggested to represent 'mounded drifts' after Rebesco et al. (2014). Their occurrence indicates focused bottom-currents along the trough floor, whose erosive nature is evidenced by the truncated reflectors of respective Units within the depressions (Fig. 5c). Conversely, the neighbouring mounds indicate enhanced sediment accumulation due to less focused flow (cf. Wilckens et al., 2023), which is especially pronounced in Units B and C at the confluence zone.

4.3. KHTS sediment ages

Radiocarbon dating shows that Units B to D and the uppermost part of Unit A are of Holocene age and cover the last ~10 ka, with the oldest age (10.2 cal ka BP; Table 3; Fig. 8) recovered from Unit A in core GeoB22058-1 in central JT. Individual units were deposited roughly simultaneously in KHT and JT (Fig. 7). The upper boundary of Unit A in JT can be constrained to 7.7–7.1 cal ka BP (GeoB22058-1 and 57–1,

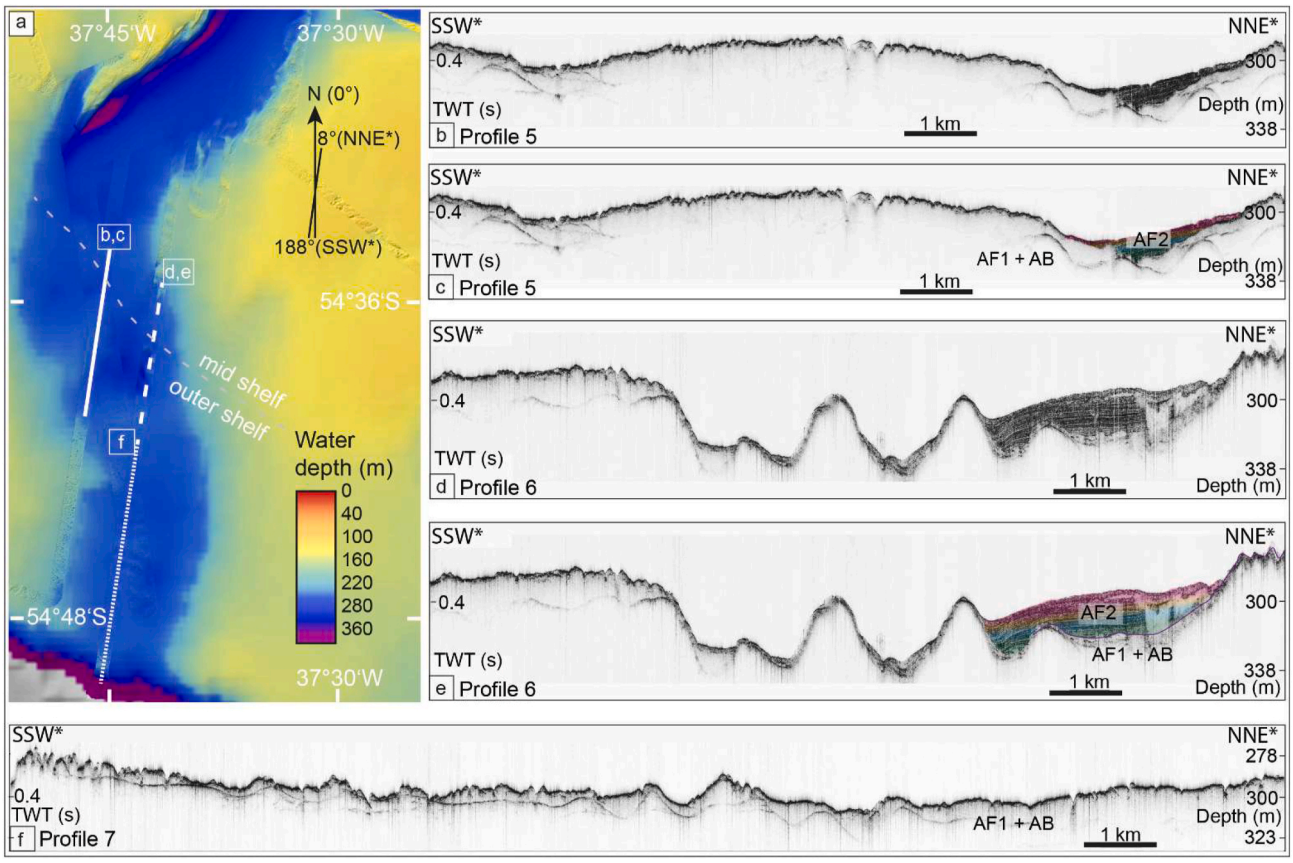

Fig. 6. a) Overview of the sub-bottom profiles on the outer shelf. b,c) Mid-to outer shelf Profile 5 and its acoustic unit interpretation. AB and AF1 mark the pre-basin-fill sequence and are subject of another paper. AF2 = Holocene trough fill with according sub-units A-D. Note the very restricted distribution of AF2 in the north-eastern part (illustrated in sub-panel c). d,e) Mid-to outer shelf Profile 6 and its interpretation of acoustic units. f) Outer shelf Profile 7. Note the complete absence of trough-fill AF2.

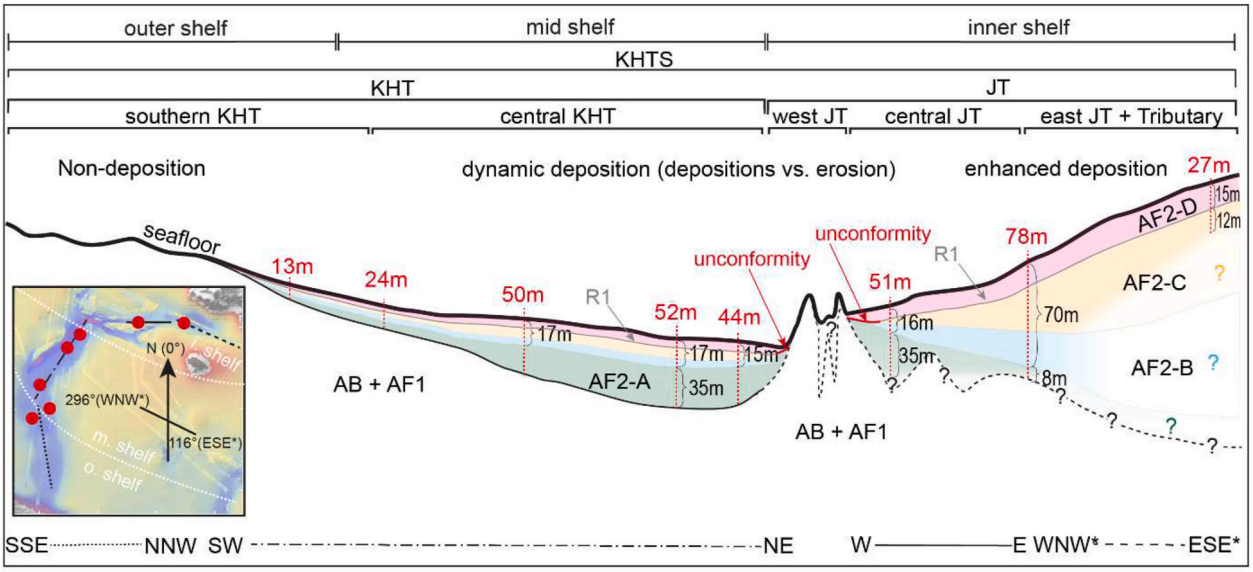

Fig. 7. Temporal and spatial variability of trough sedimentation in KHTS (not to scale). Trough-fill thicknesses are shown for individual sub-units of AF2 across a trough-wide composite sub-bottom profile. Thickness calculations are based on an average of 1500 m/s sound velocity in the sediments. Where thickness cannot be determined the approximate extent of the units is indicated by transparency and dashed lines.

respectively, Table 3) and to after 8.5 cal ka BP in KHT (PS133/2_17–13; Table 3; Fig. 8b). The overlying Unit B was deposited over the subsequent ~4 ka until ~3.9 cal ka BP in JTS (Fig. 8a), dated by GeoB22057-1. A hiatus in PS133/2_17–13 between 8.5 and 4.1 cal ka BP not only indirectly dates Unit B to this time in KHT, but also shows that a change in depositional environment at ~4 cal ka BP led to the sedimentation of

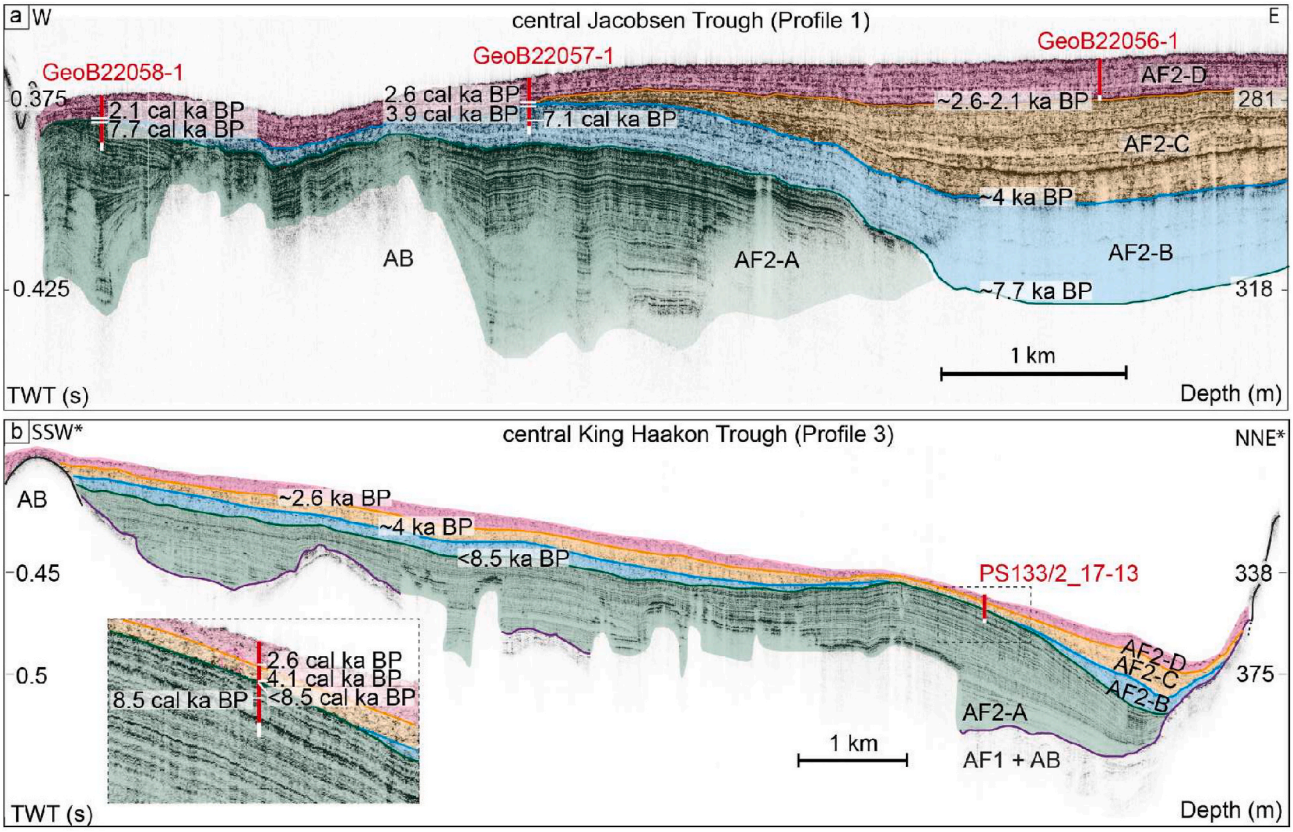

Fig. 8. a) Western part of Profile 1 from central JT (Fig. 5a). Core locations of GeoB22058-1, GeoB22057-1, GeoB22056-1 are depicted in red (true length), while white lines show possible penetration depth when accounting for 16% core compression. The calibrated radiocarbon ages closest to the unit boundaries are shown with their approximate depth in the cores. Age approximations, based on the radiocarbon ages, for the unit boundaries are indicated by ka BP. b) Profile 3 from central KHT with the core location of PS133/2_17–13 and its true length in red (possible core compression depicted in white). AB = Acoustic basement, AF1 = acoustic facies 1 (glacial till), AF2 = acoustic facies 2, i.e. glacimarine trough fill, AF2-A-D = acoustic Units A-D of AF2. (For interpretation of the references to colour in this figure legend, the reader is referred to the Web version of this article.)

Unit C (Fig. 8b). Deposition of Unit C also appears to have been simultaneous in both troughs, lasting until 2.6–2.1 cal ka BP, when the last distinct change in sedimentary environments led to the deposition of Unit D. Unit D drapes most of the trough system, and, because it is the uppermost acoustic unit, probably represents contemporary sedimentation in the study area (Fig. 7).

According to the age data, sedimentation rates have fluctuated throughout the Holocene trough-fill evolution and differ within individual units. While the core sites in central JT display either an increase or only a slight decrease in sedimentation rates across the A-B and A-D unit boundaries, sedimentation rates drop by a magnitude of 10 at the core site of PS133/2_17–13 in central KHT (Table 4). Note, however, that this might be an artefact related to the core site being located at the margin of the mounded drift (Fig. 5b and c).

5. Discussion

The seven sub-bottom profiles from KHTS show generally uniform trough-fill with mostly horizontal, conformable sediment sequences. The exception is a distinct unconformity observed in central JT (Fig. 4b and c) and in the western part of central KHT (Fig. 5d and e), as indicated by truncated upper reflectors within Units A and B. AF2 is almost entirely absent on the outer shelf, so it is likely composed of predominantly terrigenous material, sourced directly from the island. The exception are the diatom layers, which indicate a marine component, at least during the deposition of Unit A.

5.1. Timing of deposition

Based on the calibrated radiocarbon age from 388 cm beneath the erosional unconformity in central JT (GeoB22058-1; Fig. 3, Table 2), the acoustic Units B to D, as well as the uppermost part of Unit A, were deposited after ~10.2 cal ka BP. Reconstructed linear sedimentation rates would date the onset of AF2 deposition to between ~31 ka BP (151 cm ka^{-1}; max. thickness of 35 m, GeoB22058-1, Tables 2 and 4, Fig. 7) and 12.5 ka BP (873 cm ka^{-1}; max. thickness of 35 m, PS133/2_17–13, Tables 2 and 4, Fig. 7). Although an assumption of linear sedimentation rates for Unit A is unreasonable, considering the presence of contourite deposits and accordingly highly variable accumulation rates, it is feasible that deposition of AF2 initiated within this time frame. An age as old as 31 ka BP is unlikely, however, as this would imply that AF2 actually represents (sub-)glacial till from the LLGM, which is at odds with its acoustic stratification. Instead, we suggest that deposition of Unit A, i.e. AF2, initiated sometime around ~18–17 ka BP as the first marine sequence after the LLGM. This is based on two observations: (i) sediments with similar acoustic signatures as Unit A were dated to ~18 ka BP and interpreted to represent the onset of marine sedimentation in RBT (Fig. 1b; Graham et al., 2017), and (ii) the mid-shelf of the nearby Drygalski Trough (DT; Fig. 1b) remained glaciated until the onset of an early deglaciation around 17.5 cal ka BP (Lešić et al., 2022), making it unlikely that the mid-/inner shelf in KHTS was ice-free much earlier. Although it may seem odd that Unit A, even in the inner shelf regions, shows no distinct change in sedimentation pattern related to the Antarctic Cold Reversal (ACR; 14.5–12.8 ka; Jouzel et al., 1995; Putnam et al., 2010; Pedro et al., 2016; Graham et al., 2017), we actually

observed a similar pattern in outer DT (Fig. 1b; Lešić et al., 2022), where the ACR can only be identified by changes in sedimentation rates but not the types of sediments deposited (Lešić et al., 2022). Furthermore, periodic changes in ocean currents, attested to by the contourite deposits in KHTS, could have led to non-deposition or (partial) erosion of any ACR sediments. Although we consider this less likely, because ACR maximum extent was attributed to a number of outer fjord moraines around SG (Hodgson et al., 2014; Graham et al., 2017; Lešić et al., 2022) and seems unlikely to have had a large effect as far away from the active glacier margins as our core sites, we note that an onset as late as 14–12.5 ka BP is also possible. But to definitively determine the origin of Unit A, better age control from the southwestern SG continental shelf would be necessary.

The onset of deposition of Unit B occurred between 8.5 cal ka BP (PS133/2_17–13) and 7.1 cal ka BP (GeoB22057-1; Table 3; Fig. 8). Because the age from KHT derives from a depth of 126 cm below the A-B unit boundary, an age of 8.5 cal ka BP is probably slightly overestimated. Likewise, the date from GeoB22057-1 originates from right within Unit B, 304 cm below the B–C unit boundary (Fig. 8a), and thus probably significantly underestimates the onset of Unit B deposition. Since an age from just below the A-D unit boundary in GeoB22058-1 dates the uppermost 18 cm of Unit A to ~7.7 cal ka BP (Table 3, Fig. 8a), we propose that deposition of Unit B initiated between roughly 8 and ~7.7 cal ka BP, with a slight delay in JT compared to KHT, and that a change in depositional environment associated with marine erosion around this time led to the truncation of Unit A's upper reflectors in KHT (Fig. 5b,d).

Much less ambiguous are Units C and D, the onset of which is clearly dated to 4.1–3.9 cal ka BP (PS133/2_17–13, GeoB22057-1; Table 2, Fig. 8) and to 2.6–2.1 cal ka BP (GeoB22057-1, 58–1, and PS133/2_17–13; Table 2, Fig. 8), respectively. Because Unit D marks the uppermost stratigraphic unit in the acoustic data, it likely represents contemporary conditions in the trough system, although more recent changes might not have been resolved by the echosounder.

5.2. Spatial variability in sediment deposition

5.2.1. Processes controlling sedimentation in KHTS

5.2.1.1. Trough morphology and accommodation space. Glacially formed cross-shelf troughs, specifically around Antarctica, tend to flatten towards the shelf edge but slope towards the continents (Anderson et al., 1983; Dunbar et al., 1985; Klages et al., 2013), thus providing more near-shore accommodation space in land-proximal areas than close to the shelf edge. Because the sub-bottom profiler data show the same trend for central and southern KHT (Fig. 7), we suggest that the deep basins around the confluence zone between JTS and KHT, along the western flank of central KHT (Fig. 2), and in the subsurface of east JT (Fig. 4b–e), favoured sedimentation on the mid- and inner shelf. Furthermore, the deeper trough morphology in the subsurface of east JT and its spatial association with a large shear zone, the CBSZ (Fig. 2b), probably facilitated (glacial) erosion due to structural weaknesses, thus promoting larger accommodation spaces and associated sedimentation in east JT over other areas. It is noteworthy, however, that sedimentation of AF2 not only filled the deeper palaeo-relief in east JT, but also led to the accumulation of such thick sediment packages, that the seafloor slopes upwards towards the coast (Fig. 4d). This could be caused by the bottleneck-morphology of west JT (Fig. 2), which might hold back sediment within JT and cause concentrated sediment accumulation closer to the source. Nevertheless, it remains questionable why sediment continued to be held back even after the basins had been filled sufficiently to flatten the relief, which implies that trough morphology was not the only factor affecting deposition.

5.2.1.2. Sediment source. Sediment sources and their relative position to the depositional environments within KHTS likely also impacted sediment distribution. Preferential accumulation on the inner rather than on the outer shelf is consistent with distally decreasing sedimentation rates in glacimarine settings and a retreating ice-margin after maximum extent (Elverhøi et al., 1983). The rates, ranging between 34 and 873 cm ka^{-1}, compare with other glaciated continental shelves during the Holocene, e.g. Northeast Greenland (cf. Syring et al., 2020). Proximity to the sediment source could also explain the thicker sediment sequences in JT compared to central KHT, because i) more glaciers and tributaries drain the ice cap into JT (Fig. 2a) than into King Haakon Bay, together likely delivering larger amounts of sediment, ii) central KHT is further away from the feeding bay than east and central JT (Fig. 2a), and iii) King Haakon Bay (Fig. 2a) features a distinct fjord basin with an outer moraine (cf. Hodgson et al., 2014), which probably held back sediment. The remaining sediment that passed, could then have easily been deflected by along-shelf currents when entering northern KHT (Fig. 2a). In contrast, the seemingly flat morphology of Jossac Bight, Newark Bay, Jacobsen Bight and the JT tributaries, though not mapped entirely (Fig. 2a), might not have served as efficient sediment traps, but rather have permitted sediment distribution across wider areas of east and central JT (Figs. 2 and 4).

While enhanced proximal sedimentation would also be in accordance with an upward-sloping seafloor reflector towards east JT, it seems odd that the progressive thickening of AF2 within JT did not affect the entire basin-fill sequence, but only Units B-D. Although this could be an artificial effect caused by a relatively higher number of coarse grains inflating the sediment volume closer to the sediment source, differences in unit thickness also suggest that the main sedimentary processes varied over time (see section 5.3 below).

Because we derived the majority of AF2 to be supplied by SG island, Holocene sediment sources were probably fluctuating glacier margins, residual and seasonal meltwater, as well as sediment-laden run-off from rain, rivers and potential reworking processes. Accordingly, the changes between Units A-D could be related to changes in the depositional environment due to small-scale glacier fluctuations during the Holocene, triggered by climatic changes on the island (e.g. Oppedal et al., 2018; Berg et al., 2019). Although such fluctuations are unlikely to have had a significant effect on trough-wide terrigenous sediment distribution due to their restriction within the fjords (Bentley et al., 2007; Hodgson et al., 2014; Graham et al., 2017; Lešić et al., 2022), they probably still controlled sediment delivery to the inner and mid-shelf, specifically in JTS. Additionally, glacier front fluctuations could have triggered in-situ fluctuations in primary production and, accordingly, the magnitude of the biogenic fraction of the sediment, especially if meltwater served as a possible fertilisation agent (e.g. Arrigo et al., 2017), enhancing sedimentation rates during times of high primary production.

5.2.1.3. Primary productivity. Changes in biogenic content, as evidenced by the frequent occurrence of diatom layers in Unit A, indicate episodic switches between intervals with high (diatom layers) and low primary productivity (silty mud; see section 4.2). These could, incidentally, also explain the stronger acoustic stratification of Unit A in comparison to the overlying units B-D, where distinctly visible diatom layers are absent and sediment therefore might contain a larger fraction of terrigenous muds. Although these fluctuations could be related to glacier front oscillations, the presence of diatom layers in Unit A is presumed to be related to regular (predominantly siliceous) phytoplankton blooms (cf. Domack et al., 2006; Leventer et al., 2006; Graham et al., 2017). Consequently, their absence in Units B-D implies a sudden cessation of such blooms sometime after 8 and 7.7 cal ka BP in KHT and JT, respectively. Possible causes could have been reduced meltwater input and/or wind-induced mixing of the water column (Leventer et al., 2006). Alternatively, increased sediment input from the island could have "diluted" the biogenic sediment, but this seems unlikely since sedimentation rates decrease across the upper boundary of Unit A in

central KHT (PS133/2_17–13; Table 4). The regime change along the A-B unit boundary was therefore likely provoked by climatic factors that caused phytoplankton blooms to stop (see also section 5.3 below).

5.2.1.4. Shelf circulation and bottom currents. Given the dynamic behaviour of meltwater streams and ocean currents, it would be conceivable that locations of sediment accumulation vary both spatially and temporally. Indeed, variable configuration of meltwater streams and associated deposition has been documented in glacimarine settings, including fjords and continental shelves, where ocean currents additionally affect sediment distribution (e.g. Dunbar et al., 1985; Kehrl et al., 2011). Immediately after the LLGM, for instance, the establishment of a new current regime on a recently exposed continental shelf and an associated change in the depositional conditions would make sense. In fact, a similar scenario has been postulated for DT (Fig. 1b), where the progressive intrusion of (warmer) currents onto the shelf after the LLGM likely created a cavity beneath the stagnant ice margin, causing it to rapidly disintegrate from within (Lešić et al., 2022). Accordingly, retreating ice in KHTS after the LLGM could have successively exposed the shelf, while simultaneously shifting any sedimentation hotspots, generated from localised meltwater flows at the ice margin, from the outer shelf towards the coast. This is in accordance with the general trough-fill architecture that shows a shift to more island-proximal sedimentation with the onset of Unit B. Although the Holocene ages of the latter are at odds with such an interpretation, ocean currents are bound to play an important role on a shelf as wide and exposed as the one around SG. Especially during the Holocene, fluvial input from potential meltwater streams was likely decreased, making room for the more intensive pervasion of a complex system of ocean currents onto the inner shelf.

Physical oceanography observations and modelling indicate that the SG continental shelf is influenced by a number of different cross- and along shelf currents, including bottom currents, wind-induced surface currents, as well as open-ocean currents (Meredith et al., 2003, 2005; Matano et al., 2020; Combes et al., 2023). Because of SG's position in a climatically highly dynamic environment, shelf currents have been shown to change direction frequently and to impact different parts of the shelf to variable degrees. This is especially conceivable for KHTS, where a modern SACCF branch intrudes onto the continental shelf and is associated with peak along-shelf transport (Matano et al., 2020; Combes et al., 2023). Here, the complexity is probably exacerbated by a seabed characterised by deep troughs, numerous bedrock highs and several shoals, that may further affect and direct such currents (Matano et al., 2020; Combes et al., 2023). The narrow bottleneck morphology of west JT with its along-shelf west-east orientation, for instance, may have focused shelf currents flowing eastwards into the trough, thus actively preventing westward migration of island-runoff after 8 and ~7.7 cal ka BP. This would then force intensified in-situ accumulation in central and east JT, which would account for an eastward thickening of trough-fill sequences in JTS (Fig. 4). Similarly, the same SACCF-related circulation might explain limited transport of sediment into central KHT on the mid-shelf and, consequently, to southern KHT, around 8 and ~7.7 cal ka BP, as this current branch is also associated with reduced cross-shelf exchange (Matano et al., 2020).

Besides the general shelf circulation, the presence of moat-drift systems within AF2 along the western flank of KHT also indicates active bottom-currents during the Holocene (Fig. 5 b-e). In SG, where water depths rarely exceed 350 m water depth, shelf currents are probably generated and influenced by wind, tides, and thermohaline gradients. These vary seasonally and would cause bottom-currents to be less steady than those in deep water (Anderson et al., 1984; Verdicchio and Trincardi, 2008). Moreover, SG is exposed to changes in wind and temperature across the Southern Ocean, making its shelf a likely target for complex bottom-current formation. The latter is also supported by the presence of contourite drifts and associated erosional surfaces, which may, in turn, imply rather high bottom-current velocities. Nonetheless, moat development is not only dependent on current strength, but also on sediment supply (Wilckens et al., 2023). While strong currents might lead to erosion when sediment supply is low, high sediment supply can lead to aggradation within moats even at relatively high current speeds (Wilckens et al., 2023). This might be the case also in central KHT, where moats formed in the deepest areas along the (north)-western trough flank (Fig. 5b and c). Here currents are inferred to be the strongest and the most concentrated, as the Coriolis Force would deflect the SACCF to the west. In contrast, adjacent areas likely underwent preferential deposition due to decreasing currents and/or increased sediment supply (cf. Wilckens et al., 2023); the latter might be the main contributing factor, as indicated by the high sedimentation rates in Unit A.

5.3. Temporal variability in sediment deposition

In addition to the spatial variability in sediment deposition (Fig. 7), the presence of the three individual unit boundaries within AF2 suggest a temporal component to basin-fill sedimentation, which, based on coeval unit boundaries, likely affected the entire trough system (Fig. 9). Accordingly, we identify three main changes in Holocene depositional environments. The first occurred between 8 and 7.7 cal ka BP, when the diatom-rich silty muds of Unit A were replaced by the diatom-poor silty muds of Unit B and sediment deposition focused on the inner shelf. The second occurred around 4.1–3.9 cal ka BP, when silty muds of Unit C succeeded Unit B, and the third around 2.6–2.1 cal ka BP, when accumulation of the most recent Unit D began (Figs. 7, 9a-d). Interestingly, these transitions are roughly simultaneous to terrestrial climate records from SG (Rosqvist and Schuber, 2003; Oppedal et al., 2018; Berg et al., 2019; van der Bilt et al., 2022), the larger-scale Holocene climate variability reported from the Antarctic Peninsula (Bentley et al., 2009) and the South Shetland Islands (Heredia Barión et al., 2023a, 2023b), as well as Holocene SHW patterns over Patagonia (Moreno et al., 2018, 2021; McCulloch et al., 2020). This suggests a similar climatic pattern between these four regions despite a slight temporal offset in SG (Fig. 10).

5.3.1. Transition from Unit A to Unit B (around between 8 and ~7.7cal ka BP)

Unit A was characterised by relatively uniform, trough-wide deposition, strong acoustic stratification, and the intercalation of diatom layers into otherwise massive fine silty mud (Figs. 4 and 5). Because similar sediments were documented from Royal Bay Trough, this suggests relatively calm depositional conditions around large parts of SG, likely related to generally weak or absent shelf currents with limited wind-induced mixing of the water column. Nonetheless, bottom-currents must have been active enough to form the moat-drift systems in central KHT and west JT (Fig. 5c). If Unit A was indeed the first unit deposited after the LLGM, diatom blooms could have developed from seasonal discharge of fertilising meltwater from still relatively proximal glacier margins (cf. Matano et al., 2020 and references therein). Because the upper portion of Unit A dates to 10.2 to ~8 ka BP (Table 2), its deposition coincides with the Holocene Thermal Maximum (HTM; Ciais et al., 1992; Masson et al., 2000; Masson-Delmotte et al., 2004; Bentley et al., 2009). This dry and warm period occurred at the same time as a SHW minimum in Patagonia (Moreno et al., 2018, 2021), and would be in accordance with calm depositional conditions around SG (Fig. 10).

Although the HTM lasted only until ~9.5 cal ka BP in Antarctica (Ciais et al., 1992; Masson et al., 2000; Masson-Delmotte et al., 2004; Bentley et al., 2009), it prevailed until between 8 and ~7.7 cal ka BP in SG (cf. e.g. Berg et al., 2019). This time period coincides with the change from Unit A to Unit B (Fig. 9a,b, 10), whose uneven distribution shows that a trough-wide mechanism started to 'trap' sediment within JT. Trapping was accompanied by a switch to more basin-confined deposition and a change in primary production to a period where diatoms seem to have been negligible for sedimentation. Both of these

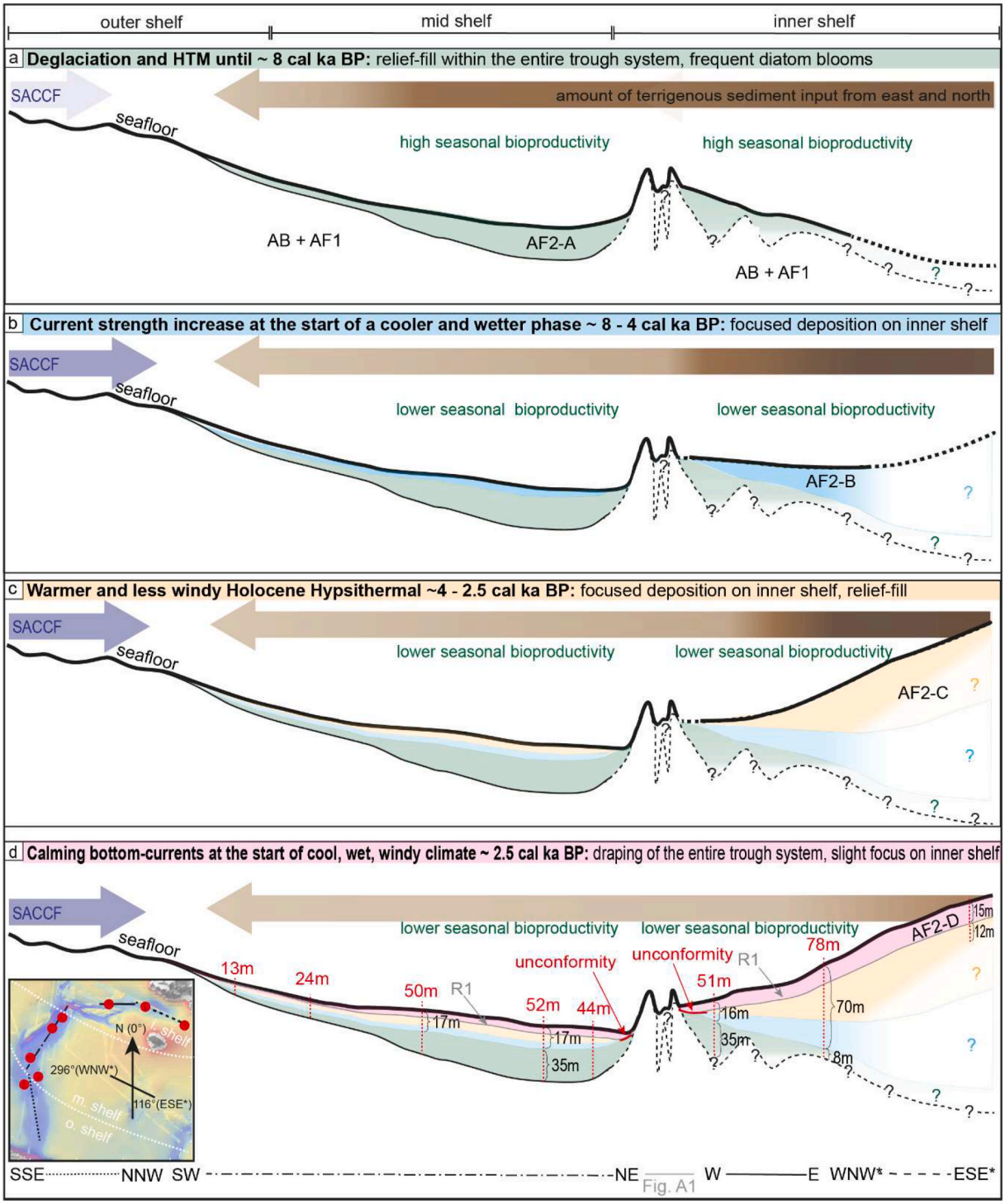

Fig. 9. a–d: Conceptual model of the evolution of the Holocene sedimentary system within KHTS, based on a composite sub-bottom profile through the trough system (not to scale). a) KHTS during the Holocene Thermal Maximum, where relatively uniform deposition of Unit AF2-A suggests increased sediment input from the island (brown arrow), coupled with enhanced marine primary productivity. Decreased influence of the Southern Antarctic Circumpolar Current Front (SACCF) is shown by the semi-transparent blue arrow. b) Uneven deposition of Unit AF2-B during the subsequent cooler and windier phase suggests sediment trapping on the inner shelf, caused by enhanced terrigenous input close to the coast (dark brown arrow) and an increasing influence in the SACCF (more opaque blue arrow). Primary productivity is much lower than before. c) KHTS during the warmer and calmer Holocene Hypsithermal and the deposition of Unit AF2-C, with similar depositional conditions as in b). d) KHTS during the last ~2.5 ka BP, where lowest input from land and marine productivity coincide with the deposition of the widespread drape of AF2-D. Red numbers refer to the visible thickness of AF2, while black numbers refer to the (composite) thickness of individual Units or Units B-D. Find the profile through west JT in the Appendix (Fig. A1). (For interpretation of the references to colour in this figure legend, the reader is referred to the Web version of this article.)

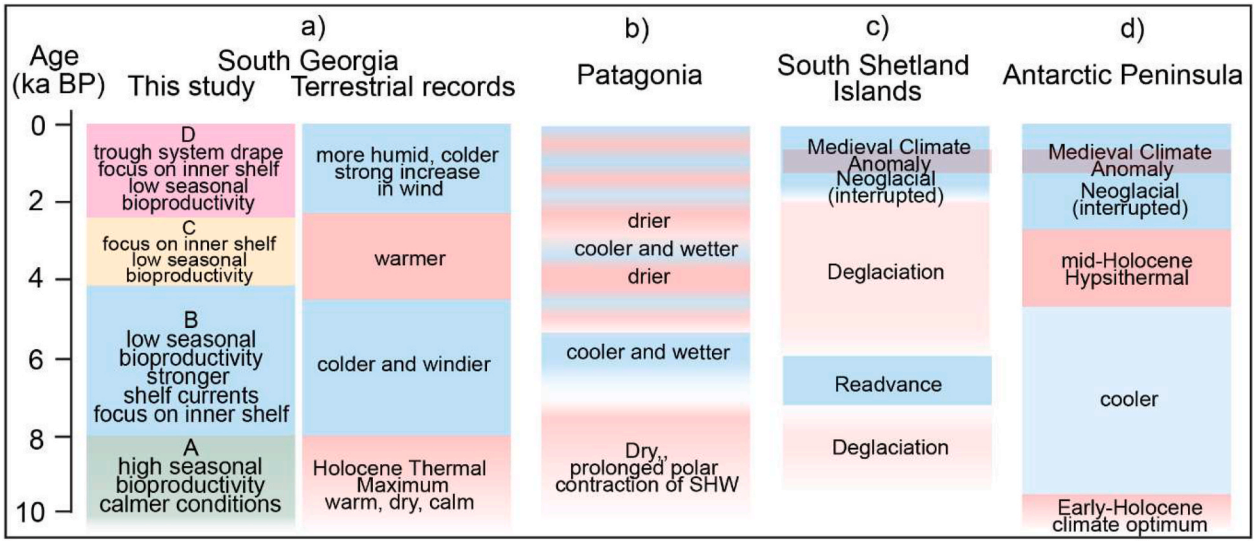

Fig. 10. Schematic visualisation of Holocene environmental changes in KHTS with respect to other areas in the sub-Antarctic. a) Sub-units of AF2 from KHTS (this study) and their comparison with Holocene climate conditions inferred from a combination of terrestrial records from northeast SG (Rosqvist and Schuber, 2003; van der Putten et al., 2004, 2009; Oppedal et al., 2018; Berg et al., 2019; Xia et al., 2020; van der Bilt et al., 2022). b) SHW-dynamic-related climate changes in Patagonia (Moreno et al., 2018, 2021; McCulloch et al., 2020), c) general glacier fluctuations and climate patterns on the South Shetland Islands (Heredia Barión et al., 2023a, 2023b) and d) the general Holocene climate pattern of the Antarctic Peninsula after Bentley et al. (2009) are also shown for comparison.

mechanisms would be in accordance with a shift from the warm HTM to generally colder conditions, which was also reported for SG's north-eastern side and Antarctica (e.g. Rosqvist and Schuber, 2003; Bentley et al., 2009; Oppedal et al., 2018; Berg et al., 2019). While sediment trapping in central and east JT might have originated in an increase in east-west directed currents, a decrease in primary production could be related to increased mixing in the water column (Leventer et al., 2006). Indeed, the SACCF may have intruded onto the continental shelf and into KHTS (Fig. 9b) as early as 8 cal ka BP (Matano et al., 2020; Combes et al., 2023), causing a change in the intensity of along-shelf currents, concurrent to a change in the strength of the SHW (cf. Gille, 2014; Liau and Chao, 2017; Yamazaki et al., 2021). The inferred reconfiguration in shelf circulation between 8 and ~7.7 cal ka BP is also in accordance with lithofacies from outer DT (Fig. 1b), where high sand content and abrupt low sedimentation rates (10 cm ka^{-1}) after 10.4 cal ka BP were interpreted to be the result of enhanced current activity on the outer shelf (Lešić et al., 2022).

A reconfiguration in shelf circulation and an associated change in bottom-currents are also indicated by the evidence for local erosion in several locations of KHTS. Truncated reflectors within the moat-drift systems along the (north-)western flank of central KHT (insets in Fig. 5c and e) suggest partial erosion of Unit A and imply sudden changes in sediment supply, sediment properties, bottom-current strength, or a combination of the three. Moreover, a smaller moat-drift system formed on top of the truncated reflectors within the already existing moat-drift system (Profile 3, Fig. 5c), and migrated laterally towards the (north-) western trough flank over time. Such migration processes are typical for moat-drift systems along bathymetric contours (Wilckens et al., 2023). Because migration continued throughout the deposition of Units B, C, and D, the change in bottom-current dynamics after 8–7.7 cal ka BP may have been long-term and caused more stable depositional conditions in KHTS throughout the remainder of the Holocene.

Truncated reflectors in central JT and west KHT are associated with a stratigraphic unconformity (Fig. 4 b,c, 8a) and might mark additional erosional events. Such events could be related to, e.g., turbidity currents, which often rework sediments on (sub-)polar continental shelves (e.g. Anderson et al., 1984; Kuvaas and Leitchenkov, 1992; Michels et al., 2001; Kuvaas et al., 2005). However, we would then expect to see other evidence of gravity-flow activity in KHTS, where both sediment cores and sub-bottom profiles lack acoustically transparent lenses and graded sediment sequences. In fact, depositional hiatuses at the respective core sites could also represent simple gaps in sedimentation, especially because it is unclear from our data (i) how many erosional events occurred, (ii) when specifically they occurred, (iii) how long they lasted, and (iv) whether sedimentation took place in between. Nonetheless, since bottom currents were the erosive agent with respect to the contourite deposits, it is feasible that such currents also affected the sedimentary sequences on a larger scale. If bottom currents travelled along their preferred west-east direction (Matano et al., 2020; Combes et al., 2023), and increased in strength after the HTM, they would have gained even more momentum upon entering west JT. The narrow bottleneck morphology would likely have caused currents to become sufficiently focused to remove the top parts of Unit A and to prevent any subsequent deposition by keeping particles in suspension. Such particles would then have been forced back towards the east, where the widening funnel-shaped morphology of central JT would have decreased the current's kinetic energy, thus causing the gradual thickening of Units B and C (Fig. 8a). Bottom currents as the responsible agent for the unconformities in KHTS are also supported by Graham et al. (2017), who interpreted an unconformity on the north-eastern shelf to derive from similar mechanisms.

5.3.2. *Transition from Unit B to Unit C (~4 cal ka BP)*

Cool and windy conditions with associated increase in bottom-current strength persisted until ~4 cal ka BP, when the onset of the Holocene Hypsithermal (Rosqvist and Schuber, 2003; Berg et al., 2019; Xia et al., 2020) marked the transition to a recurring warm period in SG and other regions of the Southern Hemisphere (Figs. 9c and 10). Small differences in acoustic properties as well as a pronounced boundary reflector between Units B and C suggest a slight shift in sedimentary processes or their magnitude around this time. Nonetheless, a climatic change around 4 ka BP must have been much less distinct than the one at the end of the HTM, as lithologies between Units B and C are remarkably similar (Lešić, unpublished data).

Assuming that the hiatus in central JT (Fig. 8a) was, in fact, caused by intensifying bottom-currents after 7.7 cal ka BP, it is likely that the hiatus between ~3.9 and 2.6 cal ka BP at site GeoB22057-1 further east was caused by similar processes (Fig. 8a). In order to account for the continued absence of Unit C in central JT (Figs. 7 and 8a), however, these currents would have had to be even stronger than the ones

establishing between 8 and ~7.7 cal ka BP. Because a further current strengthening during a transition to warmer climate seems counter-intuitive, the hiatus could alternatively be a result of an established regime of stable bottom-current conditions. These would have caused sediments to be continuously held back in the deeper basins of east JT (Fig. 9c), thus preventing their transport to more westerly regions of JT. This is supported by the pinch-out of Unit C towards site GeoB22057-1 (Fig. 4b,c, 7, 8a), suggesting decreasing accumulation of Unit C after the trough relief had been filled.

5.3.3. *Onset of trough-wide sediment draping (~2.6–2.1 cal ka BP)*

The strong bottom reflector of Unit D, *R1,* can be traced throughout the entire JTS and central KHT (Fig. 4b and c, 5 b-e) and was dated to around 2.6–2.1 cal ka BP. In addition to the regime change between 8 and ~7.7 cal ka BP, *R1* hence marks a second distinct change in depositional environments across KHTS (Fig. 9d). The draping, homogeneous character of Unit D, alongside its uniform thickness distribution, is indicative of relatively calm, open-marine conditions. A similar drape has also been reported from a sedimentary record in Cumberland Bay (Fig. 1b), where the onset of sedimentation onto a bathymetrically exposed moraine has been dated to 2.2 cal ka BP (Graham et al., 2017). This suggests that the calmer depositional conditions might have been of broader regional significance across the marine realm around SG.

Further evidence for the prevalence of calmer conditions is also given by the presence of Unit D in central JT. The fact that accumulation did take place, suggests a shift in bottom-current strength, causing the currents entering JT from the west to no longer be strong enough to reach the central trough. This is supported by the observation that Unit D started to accumulate earlier in the east (~2.6 ka BP at site GeoB22057-1) than in the west (~2.1 ka BP at site GeoB22058-1), which further implies that bottom currents might have decreased in JT.

The time frame between 2.6 and 2.1 cal ka BP coincides with a substantial change from warmer to colder and more humid conditions observed in the terrestrial regions of NE SG (2.6–2.2 cal ka BP; Fig. 10; Rosqvist and Schuber, 2003; van der Putten et al., 2004; van der Putten et al., 2009) and the start of a neoglacial in other Southern Hemisphere region (Fig. 10; Bentley et al., 2009; Moreno et al., 2018; McCulloch et al., 2020; Moreno et al., 2021; Heredia Barión et al., 2023a; Heredia Barión et al., 2023b). Indeed, this period was believed to be caused by a change to "negative Southern Annular Mode (SAM)-like conditions" (Strother et al., 2015; Zwier et al., 2021; van der Bilt et al., 2022), which are associated with a shift of low air pressure and increased winds from Antarctica to (slightly) lower latitudes (Gong and Wang, 1999; Sallée et al., 2008; Lee et al., 2019; van der Bilt et al., 2022). Accordingly, SG was reported to have experienced a general increase of the SHW and related evaporation around this time (Strother et al., 2015; Zwier et al., 2021; van der Bilt et al., 2022). Although stronger winds and enhanced evaporation seem to be at odds with our observation of more homogeneous depositional conditions and weaker/less focused bottom-currents, oceanographic models suggest that wind stress mainly affects the cross-shelf transport of the uppermost 50 m in the water column (Combes et al., 2023). Moreover, a change in strength and position of the SHW did not necessarily affect overall current strength. Instead, the SHW are a key driver of the ACC (Orsi et al., 1995) and could easily affect the prevailing oceanographic current system. We hence suggest that a change in the SHW around 2.6–2.1 cal ka BP may have caused a shift in the latitudinal position of mean ACC transport or associated frontal positions (Meredith et al., 2004; Meredith and Hogg, 2006; Sallée et al., 2008; Gille, 2014). Comparable to the shelf current reconfiguration postulated for 8 and ~7.7 cal ka BP in section 5.3.2, such a shift could then have redirected or redistributed shelf currents, causing bottom currents in JT to become less focused.

6. Conclusions

Sub-bottom profiler data, complemented with bathymetric data and selected radiocarbon ages from four sediment cores, show that a thick sequence of basin-fill sediments accumulated in KHTS throughout the Holocene. Notable differences in spatial and temporal distribution of the basin fills further imply that there was a complex interplay of factors influencing Holocene sedimentation on the southern South Georgia continental shelf. These include trough morphology and associated accommodation space, sediment sources, shelf circulation, bottom currents, marine primary productivity, as well as sediment supply from land.

The most significant transitions in the depositional environments in KHTS are marked by distinct reflectors between acoustic sub-units and occurred simultaneously to Holocene climate fluctuations between warmer and cooler phases on SG. A calm depositional environment with recurrent siliceous phytoplankton blooms due to increased meltwater input and strong stratification of the water column prevailed prior to 8 and ~7.7 cal ka BP, during the dry and warm Holocene Thermal Maximum. The end of this period was associated with a change to enhanced trapping of sediments on the inner shelf and more basin-confined sedimentation. These conditions were most likely accompanied by a shift in the position of the SACCF, leading to a reconfiguration of shelf circulation. Erosion related to focused bottom-currents in western KHT and central JT is evident from truncated reflectors of Units A and B. The subsequent deposition of Unit B, which lacks distinct diatom layers, suggests that cooler and windier conditions persisted until ~4 cal ka BP, when deposition of Unit C initiated. This transition likely marked the beginning of a recurring warmer period, the Holocene Hypsithermal, and could have been associated with a local strengthening in bottom currents through the narrow west JT, as implied by a depositional hiatus at site GeoB22057-1 in central JT. The onset of deposition of Unit D's homogeneous sediment drape was dated to around 2.6 cal ka BP and coincides with the onset of cooler climate and strong winds in the region. However, as this time period also coincides with the first sediment deposition on top of eroded portions in central JT and central KHT, it is likely that another change in SACCF position impacted shelf circulation, resulting in redirected or less focused currents in KHTS.

CRediT authorship contribution statement

Nina-Marie Lešić: Conceptualization, Data curation, Formal analysis, Methodology, Visualization, Writing – original draft, Writing – review & editing, Investigation. **Katharina Teresa Streuff:** Investigation, Supervision, Writing – review & editing. **Gerhard Bohrmann:** Funding acquisition, Project administration, Supervision, Writing – review & editing. **Sabine Kasten:** Data Curation, Writing – review & editing. **Gerhard Kuhn:** Funding acquisition, Project administration, Supervision, Writing – review & editing.

Declaration of competing interest

The authors declare that they have no known competing financial interests or personal relationships that could have appeared to influence the work reported in this paper.

Data availability

Data will be made available on request.

Acknowledgements

This publication was funded by the "Deutsche Forschungsgemeinschaft" (DFG) within the priority program SPP 1158 ″Antarctic Research with comparative investigations in Arctic ice areas" by the grants KU 683/18–1, BO 1049/23–1, and DO 705/4–1. We thank the captains and crews of RV *Meteor* cruise M134 and RV *Polarstern* cruise PS133/2 (Grant No. AWI_PS133/2_01 and AWI_PS133/2_02)

(Alfred-Wegener-Institut, 2017). We acknowledge further financial support from the Helmholtz Association (Alfred Wegener Institute Helmholtz Centre for Polar and Marine Research) and are grateful to Miriam Römer for organising the funding for participation in the Polarstern cruise via the MARUM Incentive Funds Initiative. Further, we thank the AWI core repository for providing access to gravity core PS133/2_17–13. Additionally, we thank C. Gebhardt, J. Klages, J. Wollenburg, V. Schumacher, S. Wiebe, M. Seebeck and P. Daub from the Alfred Wegener Institute, Helmholtz Centre for Polar and Marine Research in Bremerhaven, for their support. We also thank an anonymous reviewer for valuable input, which improved this contribution. Further, we thank M. Römer and N. Römer-Stange for support with SMT The Kingdom Suite and C. Ferreira for the processing of bathymetric data. All figures in this publication were created using QGIS 3.22.10 and Adobe Illustrator 2022/2023 and all maps are based on EPSG 3762.

Appendix A. Supplementary data

Supplementary data to this article can be found online at https://doi.org/10.1016/j.qsa.2023.100156.

References

Alfred-Wegener-Institut Helmholtz-Zentrum für Polar- und Meeresforschung, 2017. Polar research and supply vessel POLARSTERN operated by the alfred-wegener-institute. Journal of large-scale research facilities 3, A119. https://doi.org/10.17815/jlsrf-3-163.

Anderson, J., Brake, C., Domack, E., Myers, N., Singer, J., 1983. Sedimentary dynamics of the Antarctic continental shelf. Antarctic Earth Science 387–389.

Anderson, J.B., Brake, C.F., Myers, N.C., 1984. Sedimentation on the ross sea continental shelf, Antarctica. Mar. Geol. 57, 295–333.

Arrigo, K.R., van Dijken, G.L., Castelao, R.M., Luo, H., Rennermalm, Å.K., Tedesco, M., Mote, T.L., Oliver, H., Yager, P.L., 2017. Melting glaciers stimulate large summer phytoplankton blooms in southwest Greenland waters. Geophys. Res. Lett. 44, 6278–6285.

Bakke, J., Paasche, Ø., Schaefer, J.M., Timmermann, A., 2021. Long-term demise of sub-Antarctic glaciers modulated by the Southern Hemisphere Westerlies. Sci. Rep. 11, 1–10.

Bentley, M., Evans, D., Fogwill, C., Hansom, J., Sugden, D., Kubik, P., 2007. Glacial geomorphology and chronology of deglaciation, South Georgia, sub-Antarctic. Quat. Sci. Rev. 26, 644–677.

Bentley, M.J., Hodgson, D., Smith, J., Cofaigh, C., Domack, E., Larter, R., Roberts, S., Brachfeld, S., Leventer, A., Hjort, C., Hillenbrand, C.-D., Evans, D.J.A., 2009. Mechanisms of Holocene palaeoenvironmental change in the antarctic Peninsula region. Holocene 19, 51–69.

Berg, S., Jivcov, S., Kusch, S., Kuhn, G., Wacker, L., Rethemeyer, J., 2020. Compound-specific radiocarbon analysis of (Sub-)Antarctic coastal marine sediments - potential and challenges for chronologies. Paleoceanogr. Paleoclimatol., e2020PA003890

Berg, S., White, D.A., Jivcov, S., Melles, M., Leng, M.J., Rethemeyer, J., Allen, C., Perren, B., Bennike, O., Viehberg, F., 2019. Holocene glacier fluctuations and environmental changes in subantarctic South Georgia inferred from a sediment record from a coastal inlet. Quat. Res. 91, 132–148.

Bohrmann, G., Aromokeye, A.D., Bihler, V., Dehning, K., Dohrmann, I., Gentz, T., Grahs, M., Hogg, O., Hüttich, D., Kasten, S., Kirschenmann, E., Lange, M., Leymann, T., Linse, K., Loher, M., Malnati, J., Mau, S., Mickoleit, A., Nowald, N., Pape, T., Reuter, C., Rohleder, C., Römer, M., Sahling, H., Stange, N., Torres, M., Vittori, V., von Dobeneck, T., von Neuhoff, H., Weinrebe, W., Wintersteller, P., 2017. R/V METEOR Cruise Report M134, Emissions of Free Gas from Cross-Shelf Troughs of South Georgia: Distribution, Quantification, and Sources for Methane Ebullition Sites in Sub-Antarctic Waters, Port Stanley (Falkland Islands) - Punta Arenas (Chile), 16 January - 18 February 2017, Berichte aus dem MARUM und dem Fachbereich Geowissenschaften der Universität Bremen. MARUM–Zentrum für Marine Umweltwissenschaften, Fachbereich Geowissenschaften, Universität Bremen, pp. 1–220.

Butzin, M., Heaton, T.J., Köhler, P., Lohmann, G., 2019. Marine Radiocarbon Reservoir Ages Simulated for IntCal20. Link to Model Results in NetCDF Format, Supplement to Butzin, M., Heaton, T.J., Köhler, P., Lohmann, G., 2020. A short note on marine reservoir age simulations used in IntCal20 Radiocarbon 865–871.

Butzin, M, Heaton, TJ, Köhler, P, Lohmann, G., 2020a. A Short Note on Marine Reservoir Age Simulations Used in IntCal20. Radiocarbon 62 (4), 865–871. https://doi.org/10.1017/RDC.2020.9.

Caress, D., Chayes, D., 2017. MB-system: Mapping the Seafloor. https://www.mbari.org/products/. pp. research-software/mb-system.

Ciais, P., Petit, J., Jouzel, J., Lorius, C., Barkov, N., Lipenkov, V., Nicolaiev, V., 1992. Evidence for an early Holocene climatic optimum in the Antarctic deep ice-core record. Clim. Dynam. 6, 169–177.

Clapperton, C.M., Sugden, D.E., Birnie, J., Wilson, M.J., 1989. Late-glacial and Holocene glacier fluctuations and environmental change on south Georgia, Southern Ocean. Quat. Res. 31, 210–228.

Combes, V., Matano, R., Meredith, M., Young, E., 2023. Variability of the shelf circulation around south Georgia, Southern Ocean. J. Geophys. Res.: Oceans, e2022JC019257.

Cook, A.J., Poncet, S., Cooper, A.P.R., Herbert, D.J., Christie, D., 2010. Glacier retreat on South Georgia and implications for the spread of rats. Antarct. Sci. 22, 255–263.

Dalziel, I.W., Macdonald, D.I., Stone, P., Storey, B.C., 2021. South Georgia microcontinent: displaced fragment of the southernmost Andes. Earth Sci. Rev. 220, 103671.

Dickens, W., Kuhn, G., Leng, M., Graham, A.G., Dowdeswell, J., Meredith, M., Hillenbrand, C.-D., Hodgson, D., Roberts, S., Sloane, H., Smith, J.A., 2019. Enhanced glacial discharge from the eastern antarctic Peninsula since the 1700s associated with a positive southern annular mode. Sci. Rep. 9, 14606.

Dickens, W.A., Graham, A.G., Smith, J.A., Dowdeswell, J.A., Larter, R.D., Hillenbrand, C. D., Trathan, P.N., Erik Arndt, J., Kuhn, G., 2014. A new bathymetric compilation for the South Orkney Islands region, Antarctic Peninsula (49–39 W to 64–59 S): insights into the glacial development of the continental shelf. G-cubed 15, 2494–2514.

Domack, E., Amblas, D., Gilbert, R., Brachfeld, S., Camerlenghi, A., Rebesco, M., Canals, M., Urgeles, R., 2006. Subglacial morphology and glacial evolution of the Palmer deep outlet system, Antarctic Peninsula. Geomorphology 75, 125–142.

Dowdeswell, J., Vásquez, M., 2013. Submarine landforms in the fjords of southern Chile: implications for glacimarine processes and sedimentation in a mild glacier-influenced environment. Quat. Sci. Rev. 64, 1–19.

Dunbar, R.B., Anderson, J.B., Domack, E.W., Jacobs, S.S., 1985. Oceanographic influences on sedimentation along the Antarctic continental shelf. Oceanology of the Antarctic Continental Shelf 43, 291–312.

Elverhøi, A., Lønne, Ø., Seland, R., 1983. Glaciomarine sedimentation in a modern fjord environment, Spitsbergen. Polar Res. 1, 127–150.

Forwick, M., Vorren, T.O., Hald, M., Korsun, S., Roh, Y., Vogt, C., Yoo, K.-C., 2010. Spatial and Temporal Influence of Glaciers and Rivers on the Sedimentary Environment in Sassenfjorden and Tempelfjorden, Spitsbergen, vol. 344. Geological Society, London, Special Publications, pp. 163–193.

Foster, L.C., Pearson, E.J., Juggins, S., Hodgson, D.A., Saunders, K.M., Verleyen, E., Roberts, S., 2016. Development of a regional glycerol dialkyl glycerol tetraether (GDGT)-temperature calibration for Antarctic and sub-Antarctic lakes. Earth Planet Sci. Lett. 433, 370–379.

GEBCO Compilation Group, 2023. GEBCO 2023 Grid.

Geprägs, P., Torres, M.E., Mau, S., Kasten, S., Römer, M., Bohrmann, G., 2016. Carbon cycling fed by methane seepage at the shallow Cumberland Bay, South Georgia, sub-Antarctic. G-cubed 17, 1401–1418.

Gille, S.T., 2014. Meridional displacement of the Antarctic circumpolar current. Phil. Trans. Math. Phys. Eng. Sci. 372, 20130273.

Gong, D., Wang, S., 1999. Definition of Antarctic oscillation index. Geophys. Res. Lett. 26, 459–462.

Gordon, J.E., Haynes, V.M., Hubbard, A., 2008. Recent glacier changes and climate trends on South Georgia. Global Planet. Change 60, 72–84.

Graham, A.G.C., Fretwell, P.T., Larter, R.D., Hodgson, D.A., Wilson, C.K., Tate, A.J., Morris, P., 2008. A new bathymetric compilation highlighting extensive paleo-ice sheet drainage on the continental shelf, South Georgia, sub-Antarctica. G-cubed 9.

Graham, A.G.C., Kuhn, G., Meisel, O., Hillenbrand, C.-D., Hodgson, D.A., Ehrmann, W., Wacker, L., Wintersteller, P., Dos Santos Ferreira, C., Römer, M., White, D., Bohrmann, G., 2017. Major advance of South Georgia glaciers during the Antarctic Cold Reversal following extensive sub-Antarctic glaciation. Nat. Commun. 8, 14798.

Heaton, T., Bard, E., Ramsey, C.B., Butzin, M., Hatte, C., Hughen, K., Köhler, P., Reimer, P., 2022. A response to community questions on the Marine 20 radiocarbon age calibration curve: marine reservoir ages and the calibration of 14C samples from the oceans. Radiocarbon 1–27.

Heaton, T.J., Köhler, P., Butzin, M., Bard, E., Reimer, R.W., Austin, W.E.N., Bronk Ramsey, C., Grootes, P.M., Hughen, K.A., Kromer, B., Reimer, P.J., Adkins, J., Burke, A., Cook, M.S., Olsen, J., Skinner, L.C., 2020. Marine 20—the marine radiocarbon age calibration curve (0–55,000 cal BP). Radiocarbon 62, 779–820.

Heredia Barión, P., Roberts, S.J., Spiegel, C., Binnie, S.A., Wacker, L., Davies, J., Gabriel, I., Jones, V.J., Blockley, S., Pearson, E.J., Foster, L., Davies, S., Roland, T.P., Hocking, E.P., Bentley, M.J., Hodgson, D.A., Hayward, C.L., McCulloch, R.D., Strelin, J.A., Kuhn, G., 2023a. Holocene deglaciation and glacier readvances on the Fildes Peninsula and King George Island (Isla 25 de Mayo), South Shetland Islands, NW Antarctic Peninsula. The Holocene, 09596836231157059.

Heredia Barión, P.A., Strelin, J.A., Roberts, S.J., Spiegel, C., Wacker, L., Niedermann, S., Bentley, M.J., Pearson, E.J., Czalbowski, N.T.M., Davies, S.J., Schnetger, B., Grosjean, M., Arcusa, S., Perren, B., Hocking, E.P., Kuhn, G., 2023b. The impact of Holocene deglaciation and glacial dynamics on the landscapes and geomorphology of potter Peninsula, king george island (isla 25 mayo), NW antarctic Peninsula. Front. Earth Sci. 10, 1073075.

Hillenbrand, C.-D., Smith, J.A., Hodell, D.A., Greaves, M., Poole, C.R., Kender, S., Williams, M., Andersen, T.J., Jernas, P.E., Elderfield, H., Klages, J.P., Roberts, S.J., Gohl, K., Larter, R.D., Kuhn, G., 2017. West Antarctic Ice Sheet retreat driven by Holocene warm water incursions. Nature 547, 43–48.

Hodgson, D.A., Graham, A.G.C., Griffiths, H.J., Roberts, S.J., Cofaigh, C.Ó., Bentley, M.J., Evans, D.J.A., 2014. Glacial history of sub-Antarctic South Georgia based on the submarine geomorphology of its fjords. Quat. Sci. Rev. 89, 129–147.

Inman, D.L., Nordstrom, C.E., Flick, R.E., 1976. Currents in submarine canyons: an air-sea-land interaction. Annu. Rev. Fluid Mech. 8, 275–310.

Jouzel, J., Vaikmae, R., Petit, J., Martin, M., Duclos, Y., Stievenard, M., Lorius, C., Toots, M., Mélières, M., Burckle, L., Barkov, N., Kotlyakov, V.M., 1995. The two-step shape and timing of the last deglaciation in Antarctica. Clim. Dynam. 11, 151–161.

Kasten, S., 2023. The Expedition PS133/2 of the Research Vessel POLARSTERN to the Scotia Sea in 2022. Berichte zur Polar-und Meeresforschung= Reports on polar and marine research 775.
Kehrl, L.M., Hawley, R.L., Powell, R.D., Brigham-Grette, J., 2011. Glacimarine sedimentation processes at kronebreen and kongsvegen, svalbard. J. Glaciol. 57, 841–847.
Kirkham, J.D., Hogan, K.A., Larter, R.D., Arnold, N.S., Ely, J.C., Clark, C.D., Self, E., Games, K., Huuse, M., Stewart, M.A., Ottesen, D., Dowdeswell, J., 2022. Tunnel valley formation beneath deglaciating mid-latitude ice sheets: observations and modelling. Quat. Sci. Rev., 107680
Kirkham, J.D., Hogan, K.A., Larter, R.D., Arnold, N.S., Nitsche, F.O., Kuhn, G., Gohl, K., Anderson, J.B., Dowdeswell, J.A., 2020. Morphometry of bedrock meltwater channels on Antarctic inner continental shelves: implications for channel development and subglacial hydrology. Geomorphology 370, 107369.
Klages, J.P., Kuhn, G., Hillenbrand, C.-D., Graham, A.G.C., Smith, J.A., Larter, R.D., Gohl, K., 2013. First geomorphological record and glacial history of an inter-ice stream ridge on the West Antarctic continental shelf. Quat. Sci. Rev. 61, 47–61.
Kuvaas, B., Kristoffersen, Y., Guseva, J., Leitchenkov, G., Gandjukhin, V., Løvås, O., Sand, M., Brekke, H., 2005. Interplay of turbidite and contourite deposition along the cosmonaut sea/enderby land margin, east Antarctica. Mar. Geol. 217, 143–159.
Kuvaas, B., Leitchenkov, G., 1992. Glaciomarine turbidite and current controlled deposits in Prydz Bay, Antarctica. Mar. Geol. 108, 365–381.
Lamy, F., Kilian, R., Arz, H.A., Francois, J.-P., Kaiser, J., Prange, M., Steinke, T., 2010. Holocene changes in the position and intensity of the southern westerly wind belt. Nat. Geosci. 3, 695–699.
Lee, D.Y., Petersen, M.R., Lin, W., 2019. The southern annular mode and southern ocean surface westerly winds in E3SM. Earth Space Sci. 6, 2624–2643.
Lešić, N.-M., Streuff, K.T., Bohrmann, G., Kuhn, G., 2022. Glacimarine sediments from outer Drygalski Trough, sub-antarctic south Georgia–evidence for extensive glaciation during the last glacial maximum. Quat. Sci. Rev. 292, 107657.
Leventer, A., Domack, E., Pike, J., Stickley, C., Maddison, E., Brachfeld, S.A., Manley, P., McClennen, C., 2006. Marine sediment record from the East Antarctic margin reveals dynamics of ice sheet recession. Department of Earth and Environmental Studies FacultyScholarship and Creative Works 26.
Liau, J.-R., Chao, B.F., 2017. Variation of Antarctic circumpolar current and its intensification in relation to the southern annular mode detected in the time-variable gravity signals by GRACE satellite. Earth Planets Space 69, 1–9.
Macdonald, D.I.M., Storey, B.C., Thomson, J.W., 1987. South Georgia BAS GEOMAP Series, Sheet 1,. British Antarctic Survey, Cambridge, p. 1, 250000 Geological map and supplementary text 250063.
Masson-Delmotte, V., Stenni, B., Jouzel, J., 2004. Common millennial-scale variability of Antarctic and Southern Ocean temperatures during the past 5000 years reconstructed from the EPICA Dome C ice core. Holocene 14, 145–151.
Masson, V., Vimeux, F., Jouzel, J., Morgan, V., Delmotte, M., Ciais, P., Hammer, C., Johnsen, S., Lipenkov, V.Y., Mosley-Thompson, E., Petit, J.-R., Steig, E., Stievenard, M., Vaikmae, R., 2000. Holocene climate variability in Antarctica based on 11 ice-core isotopic records. Quat. Res. 54, 348–358.
Matano, R.P., Combes, V., Young, E.F., Meredith, M.P., 2020. Modeling the impact of ocean circulation on chlorophyll blooms around south Georgia, Southern Ocean. J. Geophys. Res.: Oceans 125, e2020JC016391.
McCulloch, R.D., Blaikie, J., Jacob, B., Mansilla, C.A., Morello, F., De Pol-Holz, R., San Román, M., Tisdall, E., Torres, J., 2020. Late glacial and Holocene climate variability, southernmost Patagonia. Quat. Sci. Rev. 229, 106131.
Meredith, M., Watkins, J., Murphy, E., Ward, P., Bone, D., Thorpe, S., Grant, S., Ladkin, R., 2003. Southern ACC front to the northeast of South Georgia: pathways, characteristics, and fluxes. J. Geophys. Res.: Oceans 108.
Meredith, M.P., Brandon, M.A., Murphy, E.J., Trathan, P.N., Thorpe, S.E., Bone, D.G., Chernyshkov, P.P., Sushin, V.A., 2005. Variability in hydrographic conditions to the east and northwest of South Georgia, 1996–2001. J. Mar. Syst. 53, 143–167.
Meredith, M.P., Hogg, A.M., 2006. Circumpolar response of Southern Ocean eddy activity to a change in the southern annular mode. Geophys. Res. Lett. 33.
Meredith, M.P., Woodworth, P.L., Hughes, C.W., Stepanov, V., 2004. Changes in the ocean transport through drake passage during the 1980s and 1990s, forced by changes in the southern annular mode. Geophys. Res. Lett. 31.
Michels, K.H., Rogenhagen, J., Kuhn, G., 2001. Recognition of contour-current influence in mixed contourite-turbidite sequences of the western Weddell Sea, Antarctica. Mar. Geophys. Res. 22, 465–485.
Mollenhauer, G., Grotheer, H., Gentz, T., Bonk, E., Hefter, J., 2021. Standard operation procedures and performance of the MICADAS radiocarbon laboratory at Alfred Wegener Institute (AWI), Germany. Nucl. Instrum. Methods Phys. Res. Sect. B Beam Interact. Mater. Atoms 496, 45–51.
Moreno, P., Henríquez, W., Pesce, O., Henríquez, C., Fletcher, M., Garreaud, R., Villa-Martínez, R., 2021. An early Holocene westerly minimum in the southern mid-latitudes. Quat. Sci. Rev. 251, 106730.
Moreno, P., Vilanova, I., Villa-Martínez, R., Dunbar, R., Mucciarone, D., Kaplan, M., Garreaud, R., Rojas, M., Moy, C., Pol-Holz, D., Lambert, F., 2018. Onset and evolution of southern annular mode-like changes at centennial timescale. Sci. Rep. 8, 1–9.
Nicholls, K.W., Østerhus, S., Makinson, K., Gammelsrød, T., Fahrbach, E., 2009. Ice-ocean processes over the continental shelf of the southern Weddell Sea, Antarctica: a review. Rev. Geophys. 47.
Nitsche, F.O., Gohl, K., Larter, R.D., Hillenbrand, C.-D., Kuhn, G., Smith, J., Jacobs, S., Anderson, J., Jakobsson, M., 2013. Paleo ice flow and subglacial meltwater dynamics in Pine Island Bay, West Antarctica. Cryosphere 7, 249–262.
Ó Cofaigh, C., 1996. Tunnel valley genesis. Prog. Phys. Geogr. 20, 1–19.
Ó Cofaigh, C., Hogan, K., Dowdeswell, J., Streuff, K., 2016. Stratified glacimarine basin-fills in West Greenland fjords. Geological Society, London, Memoirs 46, 99–100.
Oppedal, L.T., Bakke, J., Paasche, Ø., Werner, J.P., van der Bilt, W.G.M., 2018. Cirque Glacier on south Georgia shows centennial variability over the last 7000 years. Front. Earth Sci. 6.
Orsi, A.H., Whitworth, T., Nowlin, W.D., 1995. On the meridional extent and fronts of the Antarctic Circumpolar Current. Deep Sea Res. Oceanogr. Res. Pap. 42, 641–673.
Pedro, J.B., Bostock, H.C., Bitz, C.M., He, F., Vandergoes, M.J., Steig, E.J., Chase, B.M., Krause, C.E., Rasmussen, S.O., Markle, B.R., Cortese, G., 2016. The spatial extent and dynamics of the Antarctic Cold Reversal. Nat. Geosci. 9, 51–55.
Putnam, A.E., Denton, G.H., Schaefer, J.M., Barrell, D.J.A., Andersen, B.G., Finkel, R.C., Schwartz, R., Doughty, A.M., Kaplan, M.R., Schlüchter, C., 2010. Glacier advance in southern middle-latitudes during the antarctic Cold reversal. Nat. Geosci. 3, 700–704.
Rebesco, M., Hernández-Molina, F.J., Van Rooij, D., Wåhlin, A., 2014. Contourites and associated sediments controlled by deep-water circulation processes: state-of-the-art and future considerations. Mar. Geol. 352, 111–154.
Reimer, P.J., Austin, W.E.N., Bard, E., Bayliss, A., Blackwell, P.G., Ramsey, C.B., Butzin, M., Cheng, H., Edwards, R.L., Friedrich, M., Grootes, P.M., Guilderson, T.P., Hajdas, I., Heaton, T.J., Hogg, A.G., Hughen, K.A., Kromer, B., Manning, S.W., Muscheler, R., Palmer, J.G., Pearson, C., van der Plicht, J., Reimer, R.W., Richards, D.A., Scott, E.M., Southon, J.R., Turney, C.S.M., Wacker, L., Adolphi, F., Büntgen, U., Capano, M., Fahrni, S.M., Fogtmann-Schulz, A., Friedrich, R., Köhler, P., Kudsk, S., Miyake, F., Olsen, J., Reinig, F., Sakamoto, M., Sookdeo, A., Talamo, S., 2020. The IntCal20 Northern Hemisphere radiocarbon age calibration curve (0–55 cal kBP). Radiocarbon 62, 725–757.
Römer, M., Torres, M., Kasten, S., Kuhn, G., Graham, A.G.C., Mau, S., Little, C.T.S., Linse, K., Pape, T., Geprägs, P., Fischer, D., Wintersteller, P., Marcon, Y., Rethemeyer, J., Bohrmann, G., 2014. First evidence of widespread active methane seepage in the Southern Ocean, off the sub-Antarctic island of South Georgia. Earth Planet Sci. Lett. 403, 166–177.
Rosqvist, G.C., Rietti-Shati, M., Shemesh, A., 1999. Late glacial to middle Holocene climatic record of lacustrine biogenic silica oxygen isotopes from a Southern Ocean island. Geology 27, 967.
Rosqvist, G.C., Schuber, P., 2003. Millennial-scale climate changes on south Georgia, Southern Ocean. Quat. Res. 59, 470–475.
Sallée, J.B., Speer, K., Morrow, R., 2008. Response of the antarctic circumpolar current to atmospheric variability. J. Clim. 21, 3020–3039.
Seramur, K.C., Powell, R.D., Carlson, P.R., 1997. Evaluation of conditions along the grounding line of temperate marine glaciers: an example from Muir Inlet, Glacier Bay, Alaska. Mar. Geol. 140, 307–327.
Sokolov, S., Rintoul, S.R., 2009. Circumpolar structure and distribution of the Antarctic Circumpolar Current fronts: 1. Mean circumpolar paths. J. Geophys. Res.: Oceans 114.
South Georgia GIS, 2023. SGGIS.
Stow, D.A., Faugères, J.-C., Howe, J.A., Pudsey, C.J., Viana, A.R., 2002. Bottom Currents, Contourites and Deep-Sea Sediment Drifts: Current State-Of-The-Art, vol. 22. Geological Society, London, Memoirs, pp. 7–20.
Strother, S.L., Salzmann, U., Roberts, S.J., Hodgson, D.A., Woodward, J., Van Nieuwenhuyze, W., Verleyen, E., Vyverman, W., Moreton, S.G., 2015. Changes in Holocene climate and the intensity of Southern Hemisphere Westerly Winds based on a high-resolution palynological record from sub-Antarctic South Georgia. Holocene 25, 263–279.
Syring, N., Lloyd, J.M., Stein, R., Fahl, K., Roberts, D.H., Callard, L., O'Cofaigh, C., 2020. Holocene interactions between glacier retreat, sea ice formation, and Atlantic water advection at the inner Northeast Greenland continental shelf. Paleoceanogr. Paleoclimatol. 35, e2020PA004019.
Thorpe, S.E., Heywood, K.J., Brandon, M.A., Stevens, D.P., 2002. Variability of the southern antarctic circumpolar current front north of South Georgia. J. Mar. Syst. 37, 87–105.
U.S.G.S., 1981. In: Survey, U.S.G. (Ed.), U.S. Geographic Names Information System (GNIS). U.S. Geological Survey, Reston, VA.
van der Bilt, W.G., D'Andrea, W.J., Oppedal, L.T., Bakke, J., Bjune, A.E., Zwier, M., 2022. Stable Southern Hemisphere westerly winds throughout the Holocene until intensification in the last two millennia. Communications Earth & Environment 3, 1–13.
van der Putten, N., Stieperaere, H., Verbruggen, C., Ochyra, R., 2004. Holocene palaeoecology and climate history of South Georgia (sub-Antarctica) based on a macrofossil record of bryophytes and seeds. Holocene 14, 382–392.
van der Putten, N., Verbruggen, C., 2005. The onset of deglaciation of Cumberland bay and stromness bay, south Georgia. Antarct. Sci. 17, 29–32.
van der Putten, N., Verbruggen, C., Ochyra, R., Spassov, S., De Beaulieu, J.-L., De Dapper, M., Hus, J., Thouveny, N., 2009. Peat bank growth, Holocene palaeoecology and climate history of South Georgia (sub-Antarctica), based on a botanical macrofossil record. Quat. Sci. Rev. 28, 65–79.
van der Vegt, P., Janszen, A., Moscariello, A., 2012. Tunnel valleys: current knowledge and future perspectives. Geological Society, London, Special Publications 368, 75–97.
Verdicchio, G., Trincardi, F., 2008. Shallow-water contourites. Dev. Sedimentol. 60, 409–433.
Voigt, I., Chiessi, C.M., Prange, M., Mulitza, S., Groeneveld, J., Varma, V., Henrich, R., 2015. Holocene shifts of the southern westerlies across the South Atlantic. Paleoceanography 30, 39–51.
Walker, M., Johnsen, S., Rasmussen, S.O., Popp, T., Steffensen, J.P., Gibbard, P., Hoek, W., Lowe, J., Andrews, J., Björck, S., Cwynar, L.C., Hughen, K., Kershaw, P., Kromer, B., Litt, T., Lowe, D.J., Nakagawa, T., Newham, R., Schwander, J., 2009.

Formal definition and dating of the GSSP (Global Stratotype Section and Point) for the base of the Holocene using the Greenland NGRIP ice core, and selected auxiliary records. J. Quat. Sci.: Published for the Quaternary Research Association 24, 3–17.
Wilckens, H., Schwenk, T., Lüdmann, T., Betzler, C., Zhang, W., Chen, J., Hernández-Molina, F.J., Lefebvre, A., Cattaneo, A., Spieß, V., Miramontes, E., 2023. Factors controlling the morphology and internal sediment architecture of moats and their associated contourite drifts. Sedimentology 70, 1472–1495.
Xia, Z., Oppedal, L.T., Van der Putten, N., Bakke, J., Yu, Z., 2020. Ecological response of a glacier-fed peatland to late Holocene climate and glacier changes on subantarctic South Georgia. Quat. Sci. Rev. 250, 106679.
Yamazaki, K., Aoki, S., Katsumata, K., Hirano, D., Nakayama, Y., 2021. Multidecadal poleward shift of the southern boundary of the antarctic circumpolar current off east Antarctica. Sci. Adv. 7, eabf8755.
Zwier, M., van der Bilt, W.G., de Stigter, H., Bjune, A.E., 2021. Pollen Evidence of Variations in Holocene Climate and Southern Hemisphere Westerly Wind Strength on Sub-antarctic South Georgia. The Holocene, 09596836211060495.